Moona Kantele-Mesimäki

Patient on the move: feasibility of a multi-parameter respiratory rate measurement

School of Electrical Engineering

Thesis submitted for examination for the degree of Master of Science in Technology.

Espoo 11.11.2015

Thesis supervisor:

Prof. Raimo Sepponen

Thesis advisor:

D.Sc. (Tech.) Kimmo Uutela

Aalto University
School of Electrical
Engineering

AALTO UNIVERSITY
SCHOOL OF ELECTRICAL ENGINEERING

ABSTRACT OF THE
MASTER'S THESIS

Author: Moona Kantele-Mesimäki

Title: Patient on the move: feasibility of a multi-parameter respiratory rate measurement

Date: 11.11.2015 Language: English Number of pages: 8+70

Department of Electrical Engineering and Automation

Professorship: Applied Electronics

Supervisor: Prof. Raimo Sepponen

Advisor: D.Sc. (Tech.) Kimmo Uutela

Respiratory rate is one of the vital signs used to measure the body's general physical health. Abnormal respiratory rate or a change in breathing frequency may indicate deterioration in the condition of a patient. Thus, respiratory rate measurement would benefit the mobile patients on general hospital wards where no continuous monitoring exists. This environment requests wireless and reliable respiratory monitoring that would be robust against motion artefacts that impede the reliability of common respiratory rate measurements currently available.
Electrocardiography (ECG) and photoplethysmography (PPG) are common measurements in intensive care but also in sub-acute care setting. Respiration modulates the ECG and PPG waveforms in several ways that can be exploited to derive respiratory rate from these physiological signals. In ECG, the effect of breathing is seen as both amplitude and frequency modulation, whereas in PPG also baseline modulation is present.
This thesis investigated the feasibility of ECG and pulse oximetry derived respiratory rate measurements during different activities and motion states. The performances of these derived methods were evaluated together with impedance pneumography and respiratory inductive plethysmography against capnography reference using statistical analysis. A major part of this thesis consisted of the data collection, signal processing and algorithm development required to create these derived methods.
According to the results acquired, the use of ECG-derived respiration (EDR) methods based on QRS-amplitude as part of a multi-parameter respiratory rate algorithm would be feasible. However, all evaluated pulse oximetry derived respiration (PDR) methods were found to be unfit for use due to high susceptibility to motion artefacts. The development of a multi-parameter respiratory rate algorithm continues.

Keywords: respiratory rate, impedance pneumography, IP, electrocardiography derived respiration, EDR, pulse oximetry derived respiration, PDR, motion artefacts

AALTO-YLIOPISTO
SÄHKÖTEKNIIKAN KORKEAKOULU

DIPLOMITYÖN
TIIVISTELMÄ

Tekijä: Moona Kantele-Mesimäki

Työn nimi: Liikkuva potilas: moniparametrisen hengitystaajuusmittauksen käyttökelpoisuus

Päivämäärä: 11.11.2015 Kieli: Englanti Sivumäärä: 8+70

Sähkötekniikan ja automaation laitos

Professuuri: Sovellettu elektroniikka

Työn valvoja: Prof. Raimo Sepponen

Työn ohjaaja: TkT Kimmo Uutela

Hengitystaajuus luetaan yhdeksi kehon yleisestä terveydestä kertovaksi vitaaliparametriksi. Epänormaali hengitystaajuus tai hengitystaajuuden muutos voi olla merkki potilaan kunnon huononemisesta ja siksi hengitystaajuuden seurannasta olisi hyötyä myös sairaaloiden vuodeosastoilla, missä potilaat liikkuvat ilman jatkuvaa valvontaa. Tällaisessa ympäristössä hengityksen seurannan tulisi toimia langattomasti ja luotettavasti. Monet yleisesti käytetyt hengitystaajuusmittaukset kärsivät kuitenkin liikkeen aiheuttamista häiriöistä, jotka heikentävät menetelmien luotettavuutta.

Elektrokardiografia (EKG) ja fotopletysmografia (PPG) ovat yleisiä mittauksia myös tehohoidon ulkopuolella. Hengitys vaikuttaa näiden fysiologisten signaalien muotoon usealla tavalla, joita voidaan hyödyntää hengitystiedon johtamiseen näistä parametreistä. Sydänsähkökäyrän QRS-kompeksien amplitudi ja sykevälivaihtelu ovat yhteydessä hengitykseen samoin kuin fotopletysmografisen pulssiaallon perusviiva, amplitudi sekä pulssivälivaihtelu.

Tässä diplomityössä tutkittiin EKG:stä ja PPG:stä johdettujen hengitystaajuusmittausten käyttökelpoisuutta erilaisissa liiketilanteissa. Näiden johdettujen menetelmien suorituskykyä verrattiin tilastollisen analyysin keinoin impedanssipneumografian ja hengitysinduktiivisen pletysmografian kanssa kapnografialla mitattuja vertailuarvoja vastaan. Työ koostui suurelta osin myös näiden menetelmien luomiseen vaaditusta aineiston keräämisestä, signaalinkäsittelystä sekä algoritmikehityksestä. Saatujen tulosten perusteella EKG:stä johdetut amplitudipohjaiset menetelmät olisivat hyödyllisiä moniparametrisessa hengitystaajuusmittauksessa käytettynä. Sen sijaan kaikki kehitetyt PPG:stä johdetut hengitystaajuusmenetelmät todettiin käyttökelvottomiksi liikkeen aiheuttamien häiriöiden vuoksi. Moniparametrisen hengitystaajuusmittauksen kehitystyö jatkuu.

Avainsanat: hengitystaajuus, impedanssipneumografia, elektrokardiografiasta johdettu hengitys, pulssioksimetriasta johdettu hengitys, liikkeen aiheuttama häiriö

Preface

This thesis would not have been possible without the support from GE Healthcare Finland Oy and the Finnish Funding Agency for Technology and Innovation (TEKES). I have greatly enjoyed working on this topic and for that I want to express my gratitude for Engineering Manager Rene Coffeng and the whole company for giving me this opportunity. I would also like to thank Kimmo Uutela for his invaluable advice in the making of this thesis and Panu Takala for lending his expertise in impedance respiration measurements. Big thanks to Hilkka Liedes, Kari Antila and Antti Tolonen from VTT for stealing my measurement equipment and collecting the data that was crucial for the analysis. Thanks also to the parameter experts Mikko Kaski and Matti Huiku for sharing their knowledge on ECG and pulse oximetry. Thank you Hanna Viertiö-Oja for your endless enthusiasm and interest in my work. I would also like to thank the rest of the ATD team and other colleagues for making the work environment feel like home.

I would also like to take the opportunity to thank my family and friends for their love and encouragements throughout my whole life. I would most likely not be writing these words now if my parents had not in so many occasions told me that "others only do what they can, but you can do whatever you want". I will take their advice now and address my last thank you to the person that is the reason why I am so very fond of breathing: my husband Jerry.

Helsinki, 11.11.2015

Moona Kantele-Mesimäki

Contents

Abstract ii

Abstract (in Finnish) iii

Preface iv

Contents v

Symbols and abbreviations vii

1 Introduction 1

2 Background 3
2.1 Pulmonary physiology . . . 3
2.1.1 Structure of the respiratory system . . . 3
2.1.2 Function of the respiratory system . . . 5
2.1.3 Lung volumes . . . 6
2.1.4 Mechanics of the lung . . . 8
2.1.5 Abnormalities in pulmonary function . . . 9
2.2 Non-invasive measurements of respiratory rate . . . 10
2.2.1 Capnography . . . 11
2.2.2 Impedance pneumography . . . 12
2.2.3 Respiratory inductive plethysmography . . . 15
2.2.4 Other methods . . . 16
2.3 Detecting movements with accelerometers . . . 17
2.4 Deriving respiration from other physiological measurements . . . 19
2.4.1 Electrocardiography . . . 20
2.4.2 Pulse oximetry . . . 24
2.5 Motion artefacts . . . 27

3 Materials and methods 29
3.1 Data collection . . . 29
3.1.1 Measurement equipment . . . 29
3.1.2 Test protocol . . . 30
3.1.3 Volunteers . . . 30
3.2 Algorithm development . . . 31
3.2.1 Signal preprocessing . . . 31
3.2.2 ECG-derived respiration methods . . . 32
3.2.3 Pulse oximetry derived respiration methods . . . 33
3.2.4 Respiratory rate calculation . . . 35
3.3 Algorithm evaluation . . . 36
3.3.1 Performance measures . . . 36
3.3.2 Effect of different activities . . . 38

4 Results **39**
4.1 Algorithm performance evaluation 40
4.1.1 Reliability 41
4.1.2 Bias 42
4.1.3 Accuracy 43
4.1.4 Precision 44
4.1.5 Correlation 45
4.1.6 Overall performance of evaluated methods 46
4.2 Activity evaluation 47
4.2.1 Reliability 48
4.2.2 Alarm performance 50
4.2.3 Prediction probabilities 52
4.3 Reliability of acquired results 52

5 Conclusions **55**

References **57**

A Test protocols **65**

Symbols and abbreviations

Symbols

A	area
a	magnitude of acceleration
C	compliance, elastic property of the lung
D	diffusion coefficient
f	threshold factor
I	current
l	length of airway
P	partial pressure
ΔP	pressure difference (P_1 - P_2)
$P_{A,X}$	alveolar partial pressure of X
$P_{a,X}$	arterial partial pressure of X
Q	flow
$\dot{Q}_c$	capillary perfusion
$\hat{Q}_3$	third quartile
R	airway resistance
r	radius of airway
t	thickness of membrane
U	voltage
V	volume
ΔV	change in volume
$\dot{V}_A$	alveolar ventilation
$\dot{V}_D$	rate of diffusion, volume of diffusing gas
Z	impedance
η	viscosity

Abbreviations

AC	alternating current
ACC	accelerometer
Amp	amplitude
BPF	band-pass filter
brpm	breaths per minute
C	chest lead, non-standard
CA	cardiac angle
CO_2	carbon dioxide
DC	direct current
DV	dead volume, anatomical deadspace
ECG	electrocardiography
EDR	ECG-derived respiration
EMD	empirical mode decomposition
FFT	fast Fourier transform
HRV	heart rate variability
IMF	intrinsic mode function
IP	impedance pneumography
MV	minute volume
O_2	oxygen
PCA	principal component analysis
PDR	pulse oximetry derived respiration, PPG-derived respiration
PPG	photoplethysmogram
RIP	respiratory inductive plethysmography
RR	respiratory rate
RSA	respiratory sinus arrhythmia
SD	standard deviation
SpO_2	oxygen saturation of arterial blood monitored by pulse oximetry
TV	tidal volume

1 Introduction

The deterioration of hospitalized patients on general wards too often remains unnoticed due to the lack of frequent monitoring [1]. Early recognition of deteriorating patients and appropriate reaction are considered key elements in reducing the number of unexpected deaths, cardiac arrests and other severe adverse events [2, 3, 4]. Often patient deterioration is preceded by abnormalities in vital signs several hours prior to the event [2, 5]. Thus, frequent assessment of patient's vital signs could promote early recognition.

Different track and trigger systems, such as the early warning score, track the patient's condition by calculating a score based on the patient's vital signs, and also trigger response from critical care experts when the assigned score exceeds a predefined threshold. These track and trigger systems often monitor respiratory rate (RR), heart or pulse rate, blood pressure, oxygen saturations (SpO_2), temperature, and level of consciousness. There is a consensus among experts that all hospitalized patients require monitoring of these physiological parameters [6]. Naturally, increasing the frequency of vital sign measurements quickens the detection of patient deterioration. Automated and continuous vital sign measurements can improve patient safety also in the general wards [7].

Many studies have suggested that RR is one of the best indicators for adverse events [2, 8, 9], but the importance of the parameter is often overlooked [10]. In some situations, for example after myocardial infarction, an elevated RR predicts a significantly worse outcome, and a rise of 4 breaths per minute (brpm) doubles the risk [11]. Thus, monitoring of RR is important and the reliability of the measurement can be critical. Regardless of its significance, RR alone does not provide information about the adequacy of ventilation. Identification of hypoventilation or hyperventilation requires the knowledge of minute ventilation (MV), which is the product or both RR and tidal volume (TV).

Unexpected in-hospital deaths can be characterized by three distinct patterns: hyperventilation compensated respiratory failure, carbon dioxide narcosis, and arousal failure after repetitive apnea [15]. Monitoring SpO_2 alone often fails to detect early enough the respiratory changes associated with these types of respiratory failures. All three types of respiratory failure leading to unexpected death could potentially be identified by monitoring changes in MV over time combined with apnea detection. A reliable and robust RR calculation method is a key component of such respiratory monitoring solution.

When a patient is unintubated, as they usually are in the general wards, RR is often measured by impedance pneumography (IP), if it is measured at all. However, IP is unable to detect some detrimental respiratory conditions, such as obstructive apnea, due to the limitations in differentiating between true breaths and attempts to breathe [12, p. 109]. Although a significant drop in SpO_2 indicates inadequate supply of oxygen to tissues and consequently problems in respiration, SpO_2 values below 90% are regarded as late indicators of patient deterioration [13], but are still common in patients with chronic lung disease, including chronic obstructive pulmonary disease [14]. Nevertheless, the most important challenge with IP is its

susceptibility to motion artefacts when the patient moves. In addition to IP, many other respiratory rate measurements exist, but the most accurate ones are poorly suited to ambulatory environment. Hence, improving the reliability and robustness of RR measurement could facilitate early recognition of the deteriorating patients and potentially decrease the number of severe adverse events occurring on general hospital wards.

This thesis investigates the feasibility of a multi-parameter respiratory rate measurement using data sources easily available in the sub-acute care setting, namely electrocardiography (ECG), pulse oximetry, and accelerometry. These physiological measurements contain information about respiration that can be utilized to derive RR from these signals. In this thesis, existing methods deriving RR from ECG and the photoplethysmographic (PPG) waveform are studied and implemented. The aim is to answer the question whether the multi-parameter methods developed here are feasible in calculating respiratory rate during different activities and motion states. Other study questions include identifying the conditions when IP is unreliable and assessing whether ECG-derived respiration (EDR) or pulse oximetry derived respiration (PDR) are able to perform better in these situations. The final objective is to improve the reliability of RR measurement during different activities by utilizing multiple sources of clinical information in order to create a solution that is robust also in the presence of motion.

Chapter 2 contains a review of current literature and explains how the respiratory system works, how respiration can be measured, and how respiratory information can be derived from common physiological signals. Chapter 3 describes the practical engineering work done for this thesis, including data collection, signal processing, and algorithm development and evaluation. Results of the data analysis are presented and discussed in chapter 4. Finally, conclusions are drawn in chapter 5.

2 Background

Adequate supply of oxygen (O_2) is vital to human organs and their function. Human cells produce energy, water and carbon dioxide (CO_2) by consuming oxygen and glucose in a process called cellular respiration. In physiology, the term respiration refers to the intake and transport of O_2 from inhaled air to tissues, and the removal and transport of CO_2 in the opposite direction. Monitoring of respiratory function enables the detection of deficient breathing which can prove to be fatal if not acted upon in time.

This chapter is divided into five sections. The first section covers both anatomy and function of the respiratory system as well as some malfunctions in breathing. The second section describes different methods of measuring respiratory function in terms of respiratory rate and tidal volume. The third section provides an overview of the use of accelerometers in detecting movements, including respiratory movements. The fourth section investigates the possibilities of utilizing ECG and PPG to calculate respiratory rate, and the final section discusses the challenges associated with motion.

2.1 Pulmonary physiology

The main task of the respiratory system is to provide oxygen for cellular metabolism and to remove the metabolic waste product, carbon dioxide. Furthermore, the acid base balance, i.e. the pH of the body, is regulated by respiration and removal of CO_2. The basics of pulmonary physiology are summarized in this section.

2.1.1 Structure of the respiratory system

The respiratory system consists of the upper and lower respiratory tract, the rib cage, the muscles of ventilation, the blood or perfusion system, and the control system [12, p. 2-3]. The upper and lower respiratory tract are depicted in Figure 1. The upper respiratory tract consists of nasal and oral cavity, pharynx, and larynx, while the trachea and lungs constitute the lower respiratory tract. The main inspiratory muscle is the diaphragm. The other primary muscles of ventilation, the external and internal intercostal muscles, run between the ribs and assist in breathing when more effort is needed. The perfusion system consists of the pulmonary capillaries, and in a wider sense also the heart and the whole vascular system delivering blood to the lungs. The control system contains the central nervous system and peripheral nerves innervating the ventilatory muscles.

During inhalation, the air flows through the oral or nasal cavity into the pharynx and through the open epiglottis into trachea which divides into two main bronchi. The trachea and bronchi are cartilaginous airways. The right bronchus continues downwards while the left bronchus changes its course more sideways to make room for the heart. The right bronchus branch into three lobar bronchi – superior, middle, and inferior bronchi – that conduct air into the three lobes, respectively. The left lung has only two lobar bronchi and two lobes because of the location of the heart between the lungs. The lobar bronchi further branch over 20 times into thinner membranous

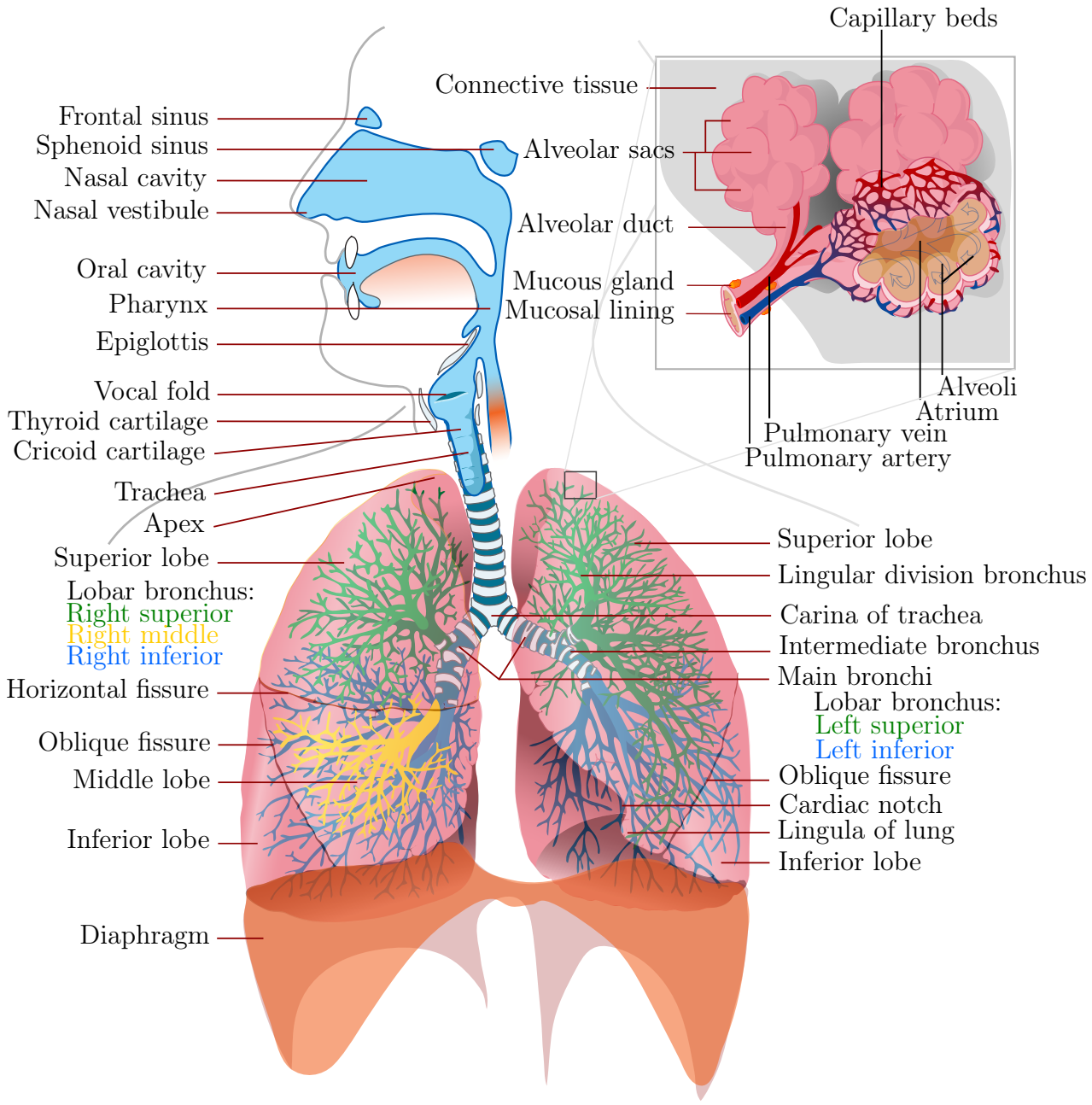

Figure 1: Respiratory system. Modified from Wikimedia Commons.

bronchioles completing the tracheobronchial tree. The terminal bronchioles open into alveolar sacs and the alveoli through the alveolar duct. The alveolar walls are covered in capillaries formed by pulmonary venules and arterioles. [12, p. 5-7]

The lungs are confined in the thoracic cavity by the rib cage and the diaphragm. The lungs and the inner wall of the thoracic cavity are lined by a double layer of thin tissue called pleura. The space between the two pleurae, the pleural cavity, contains fluid that acts as lubricant to reduce friction during the movement of the lungs at respiration.

2.1.2 Function of the respiratory system

Active work by the inspiratory muscles is required to draw air into the lungs. The movement of gases into and out of the lungs is called ventilation. During inhalation, the diaphragm moves down towards the abdomen, which enlarges the volume of the thoracic cavity and creates subatmospheric pressure that makes air flow into the lungs. As air fills the lungs the alveoli expand. During exhalation, the diaphragm relaxes and returns back to its original position decreasing the thoracic volume and creating pressure in the lungs that pushes the air out through the conductive airways as the alveoli deflate. The diaphragm is innervated via the right and left phrenic nerves and controlled by the central nervous system [12, p. 11].

The upper respiratory tract filters the air and adds heat and moisture to inhaled air and recovers them from expired gases. The conductive airways, including nose, throat and trachea, do not participate in gas exchange, which takes place in the alveoli. In addition to the alveoli, the gas exchange region contains also the respiratory bronchioles and alveolar ducts. [12, p. 5-9]

The gas exchange is based on passive diffusion across the alveolar capillary membrane and happens in the direction of concentration gradient, i.e. from higher to lower concentration. Therefore, oxygen diffuses into capillaries from the inhaled air whereas carbon dioxide diffuses from blood to lungs and out of the body via exhalation. The partial pressures of oxygen (P_{O_2}) and carbon dioxide (P_{CO_2}) are presented in Figure 2. The difference in oxygen concentration between alveoli and blood entering the lungs is approximately 60 mmHg and acts as the driving force for diffusion. In an optimal situation, the partial pressure of oxygen in alveolar capillaries (P_{a,O_2}) after diffusion would equal the partial pressure in alveoli (P_{A,O_2}), but often a small difference of less than 5 mmHg remains. Thus, it can be concluded that the partial pressure of oxygen in blood leaving the lungs is approximately 100 mmHg. [12, p. 24-31]

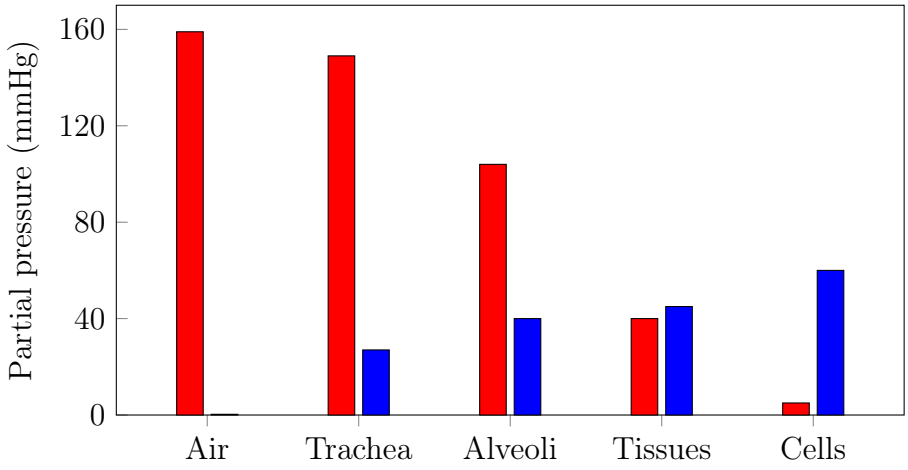

Figure 2: Partial pressures of oxygen (red) and carbon dioxide (blue).

The rate of diffusion can be expressed as Fick's law

$$\dot{V}_D = \frac{AD(P_1 - P_2)}{t}, \tag{1}$$

where $\dot{V}_D$ is the rate of diffusion in ml/min, A is the surface area of the diffusion membrane, D is the diffusion coefficient, P_1-P_2 is the partial pressure difference across the membrane, and t is thickness of the membrane. Perfusion is a prerequisite for diffusion, and refers to the blood flow through the capillaries. Without perfusion there would be no blood for the oxygen to diffuse into.

Perfusion is maintained by the pulmonary circulation. The right heart pumps blood into the pulmonary artery which branches into smaller arterioles and finally alveolar capillaries where the blood is oxygenated. The capillaries connect to pulmonary venules leading to pulmonary veins and back to the heart. The left heart delivers the oxygenated blood into all tissues of the body where cellular metabolism consumes oxygen and produces carbon dioxide. The systemic circulation returns the oxygen-deprived blood to the right heart to be pumped into the lungs again.

Oxygen is carried in the circulation by hemoglobin molecules, but a small amount is also dissolved in blood. Carbon dioxide can be carried in either the plasma or the red blood cells. The majority of CO_2 is carried as bicarbonate (HCO_3^-), while about 5-10% is dissolved as such and approximately a quarter is combined with proteins. The blood contains more than twice as much carbon dioxide compared to oxygen, 48 ml of CO_2 against 20 ml of O_2 in 100 ml of blood. [12, p. 35-39]

The respiratory control system monitors concentrations of oxygen, carbon dioxide and hydrogen ions. Ventilation can be controlled both voluntarily from the cerebral cortex and involuntarily from the medulla of the brain stem. The regulation of ventilation is based on multiple sensory feedback mechanisms, including both chemical and mechanical sensors. The central chemoreceptors located in the medulla detect only changes in pH. A rise in pH is an indirect effect of increased P_{CO_2}, which triggers the medulla to send a command to increase TV and RR. There are also peripheral chemoreceptors in the aortic arch and in the bifurcation of the common carotid artery which monitor primarily the oxygen level but also carbon dioxide and hydrogen levels. These receptors induce changes in TV and respiratory drive. The mechanoreceptors located in the airways and lungs provide the respiratory control centre with information about irritation, stretch and capillary congestion. [12, p. 41-45]

2.1.3 Lung volumes

The volume of the lungs changes during ventilation. Total lung capacity (TLC) for a normal adult is 6 litres. However, this volume cannot be fully utilized, because the lungs cannot be emptied to zero volume. On average, 1.5 litres remain in the lungs even after forced exhalation, a volume referred to as the residual volume (RV). The volume of one normal breath typically equals half a litre and is called the tidal volume (TV). The amount of air that can be inhaled after a normal breath is called the inspiratory reserve volume (IRV). Correspondingly, the amount or air that can

still be exhaled after a normal exhalation is called the expiratory reserve volume (ERV). IRV is typically about 2.5 litres while ERV is about 1.5 litres. The sum of TV, IRV and ERV is the volume that can be controlled and is called the vital capacity (VC). TLC can also be divided into inspiratory capacity (IC) and functional residual capacity (FRC). IC equals the maximal volume of inhalation after a normal exhalation whereas FRC refers to the sum of RV and ERV. [12, p. 11-13] These lung volumes and capacities are presented in Figure 3.

Minute volume (MV), the volume of air that is inhaled during one minute, can be calculated by multiplication or RR and TV.

$$MV = RR \times TV. \tag{2}$$

However, not all of TV participates in gas exchange. The volume of the conductive airways is referred to as the anatomical deadspace (DV) which equals approximately 150 ml on an adult. Therefore, the true volume available for gas exchange, alveolar ventilation ($\dot{V}_A$), is calculated by

$$\dot{V}_A = RR \times (TV - DV). \tag{3}$$

Thus, the same MV can result from two very different situations where $\dot{V}_A$ differs significantly. For example, RR 30/min and TV 200 ml, and RR 12/min and TV 500 ml both correspond to MV of 6 litres, while $\dot{V}_A$ corresponds to 1.5 litres and 4.2 litres, respectively.

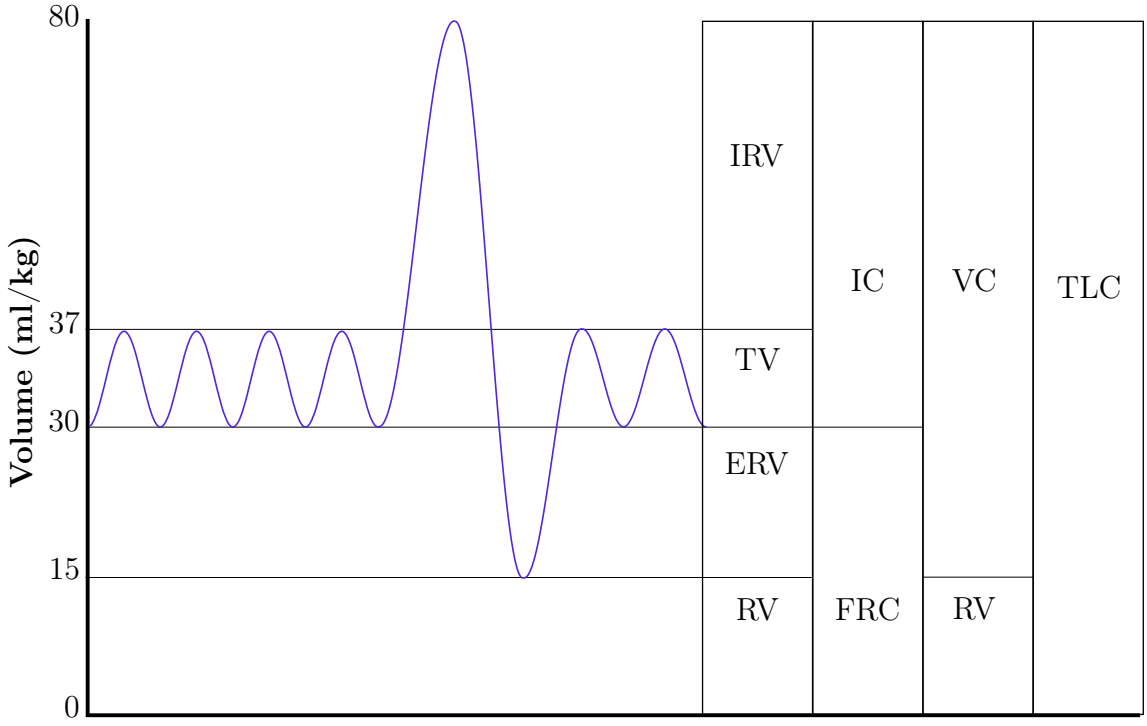

Figure 3: Lung volumes and capacities as seen in a spirograph of a normal person taking 4 tidal breaths before maximal inspiration and expiration. Modified from Wikimedia Commons.

2.1.4 Mechanics of the lung

Lung mechanics are often described by two properties, resistance and compliance. Resistance is linked to the work required to move air in and out of the lungs and is mostly caused by the conducting airways. Compliance, on the other, is related to the distensibility of the lung and is a property of the gas exchange region. Compliance is a static feature as it requires no air flow whereas resistance is a dynamic property. [12, p. 15-19]

Force is needed to expand the alveolar walls. Compliance represents the elasticity of the lung in terms of pressure change (ΔP) needed to induce a certain change in lung volume (ΔV). Mathematically, compliance is expressed as

$$C = \frac{\Delta V}{\Delta P}. \tag{4}$$

A number of different compliances can be defined, including lung compliance, chest wall compliance, and respiratory system or total compliance, which is often calculated by dividing TV by the difference between the pressure during inspiratory pause (plateau) and at the end of expiration (baseline) as expressed in Equation 5. The plateau pressure represents the elastic forces of the system.

$$\text{Respiratory system compliance} = \frac{TV}{P_{Plateau} - P_{Baseline}} \tag{5}$$

A compliant lung is one that requires only little pressure to inflate, while a non-compliant lung demands a large pressure. [12, p. 16] The compliance of the lung may be altered by pulmonary diseases and other factors. A decrease in compliance requires more effort to inhale a normal volume of air, whereas an increase in compliance makes it harder to exhale.

Ventilation requires the resistance of conductive airways against air flow be overcome by a pressure difference. Resistance can be expressed as

$$R = \frac{\Delta P}{Q}, \tag{6}$$

where ΔP is the difference between inspiratory peak pressure and plateau pressure, and Q is air flow. Air flow can be calculated from Poiseuille's law

$$Q = \frac{(\Delta P)\pi r^4}{8l\eta}, \tag{7}$$

where r is the radius and l is the length of the airway and η is viscosity. Combining Equations 6 and 7 gives

$$R = \frac{8l\eta}{\pi r^4}. \tag{8}$$

Equation 8 shows that the radius of the airway has a major effect on airway resistance. Changes in the radius of the airway have a significant impact on airway resistance. Increased airway resistance causes more laborious breathing, and can be the result of bronchoconstriction, mucosal irritation or swelling, thickening of the mucosal layer, or airway compression. [12, p. 17-19]

2.1.5 Abnormalities in pulmonary function

If the function of the respiratory system is disturbed the concentrations of arterial oxygen and carbon dioxide may change as well as TV and RR. Impaired gas exchange can arise from a decrease or lack of ventilation, perfusion or diffusion.

Inefficient ventilation, or hypoventilation, is caused by a decrease in respiratory frequency or volume, or both. Hypoventilation may result from damage to the neuronal pathways controlling respiration or weakened function of the ventilatory muscles[16, p. 25]. Hypoventilation causes the alveolar P_{O_2} to drop (alveolar hypoxia) and arterial P_{CO_2} to rise above normal (hypercapnia). Alveolar P_{O_2} sets the upper limit of arterial P_{O_2}, which means that a low P_{A,O_2} also results in low P_{a,O_2}. [17, p. 182]

Typically, it is perfusion rather than diffusion that limits the amount of oxygen intake [12, p. 23-25]. However, hypoperfusion may result from low cardiac output [17, p. 185] or a local decrease in blood flow, for example in the case of a pulmonary embolism, a mass travelling in the circulation blocking a pulmonary artery [16, p. 24]. Diffusion impairment may result from the thickening of the alveolar capillary membrane, for example in pulmonary edema, which is a condition causing accumulation of fluid in the lung [12, p. 33].

Sometimes a part of the lungs may be perfused but not ventilated, or vice versa. Pulmonary shunts decrease the arterial P_{O_2}, since shunted blood does not come into contact with alveolar gas. An alveolus belongs to the functional deadspace if it is ventilated but not perfused. Often impaired gas exchange is caused by ventilation-perfusion imbalance. The relationship between ventilation and perfusion can be characterized by ventilation-perfusion ratio ($\dot{V}_A/\dot{Q}_c$). [17, p. 184] A ratio of 0 corresponds to zero ventilation or a shunt, while an infinite ratio is related to non-existent perfusion, i.e. deadspace. A normal $\dot{V}_A/\dot{Q}_c$ varies between 0.8 and 1. The ratio is usually higher in the upper part of the lungs and slightly lower in the base of the lungs, because there is some more blood flow in the lower parts of the lungs due to gravity, and the upper parts of the lungs are over-ventilated in relation to their perfusion. [12, p. 33-34]

In chronic obstructive pulmonary disease (COPD), obstructions in the airways increase airway resistance. To compensate for the increased resistance, COPD patients tend to keep their lungs inflated, in the state of hyperinflation. Correspondingly, other conditions, such as obesity, may decrease lung volumes, especially ERV. Diseases of the lung tissue also decrease TLC and VC as well as compliance. [16, p. 23-24]

Abnormalities in RR or TV are clinically significant only when they result in insufficient gas exchange. A change in RR or TV does not automatically indicate a disturbance in respiration but can be a valid response to increased or decreased oxygen demand, a sign of well-functioning control of respiration. Thus, monitoring only RR or TV does not necessarily allow drawing conclusions about the efficiency of breathing in terms of oxygen and carbon dioxide balance.

Oxygen saturations can be monitored by pulse oximetry and give a good estimate of oxygenation and the efficiency of breathing. However, in the most common pattern of unexpected in-hospital death, oxygen saturation stays constant until it suddenly

starts to drop rapidly, at which point chances of survival are decreased regardless of emergency intervention [15]. This type of instability leading to death is associated with a rise in minute ventilation and requires monitoring of both RR and TV in order to be detected in time.

Table 1 summarises different respiratory conditions and disturbances.

Table 1: Summary of terminology for respiratory conditions

Cessation of breathing	
Apnea	temporary cessation of breathing
Respiratory arrest	total cessation of breathing
Abnormal RR or TV	
Bradypnea	abnormally low RR
Tachypnea	abnormally high RR and low TV
Hyperpnea	abnormally high TV
Hypopnea	abnormally low TV
Efficiency of ventilation	
Hyperventilation	abnormally high RR or TV, overly efficient ventilation, abnormally low P_{CO_2}
Hypoventilation	abnormally low RR or TV, inefficient ventilation, abnormally high P_{CO_2}
Other respiratory conditions	
Hypercapnia	abnormally high P_{a,CO_2}, caused by hypoventilation
Hyperinflation	abnormally fully inflated lungs throughout ventilatory cycle, caused by increased resistance
Hypoperfusion	abnormally low rate of perfusion
Hypoxia	abnormally low P_{a,O_2}, caused by hypoventilation

2.2 Non-invasive measurements of respiratory rate

Respiration can be directly monitored by measuring the amount of air entering and leaving the lungs. Spirometry, the direct measurement of respiratory volume and flow can be used to monitor respiratory rate. However, this kind of measurement requires equipment inconvenient for continuous use.

This thesis focuses on monitoring respiration of adult mobile patients in hospital general wards. In this patient population, all monitoring equipment should be non-invasive and allow the patient to move without compromising patient safety and reliability of measurements. For this reason, direct measurements are not ideal and there exists multiple indirect methods capable of monitoring respiratory rate.

2.2.1 Capnography

Capnography refers to the measurement of inhaled and exhaled carbon dioxide concentrations in the airway and also to the graphical representation of the CO_2 waveform, capnogram. A capnogram over five respiratory cycles is shown in Figure 4. There are two types of capnographs: mainstream and sidestream. [18, 12] In mainstream capnography, the CO_2 detector is usually connected to an endotracheal tube, whereas in sidestream capnography the detector is inside the monitor and a separate sampling line is required to conduct the gas samples into the detector site, where CO_2 is often detected by infrared absorption. [18]

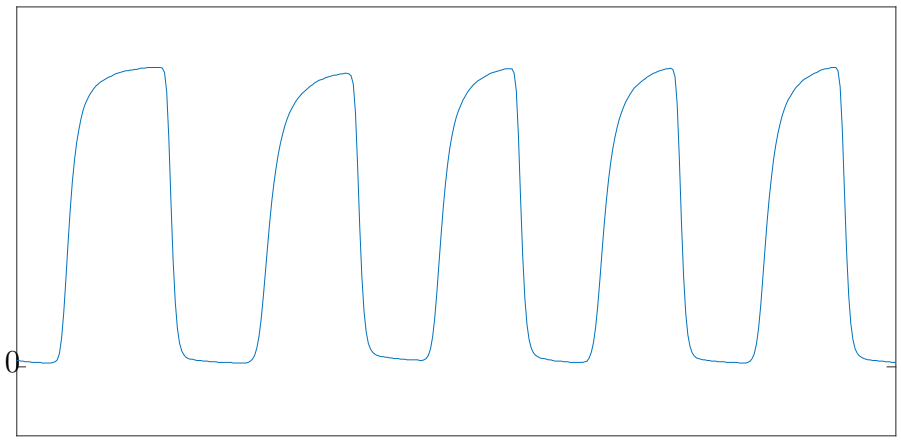

Figure 4: Capnogram over five breathing cycles.

Extubated and spontaneously breathing patients must use a breathing mask so that it does not matter whether the patient is breathing through the nose or mouth. Nasal cannula can of course be used, but then the patient should be instructed to breathe through the nose as any gas expired through the mouth will not be sampled. This applies to all respiratory measurements that require expiratory gas sampling. Wearing a breathing mask or nasal cannula over long periods of time can also be uncomfortable and lead to the removal of the mask or nasal cannula, which interrupts the measurement. This is why capnography is not optimal for ambulatory patients. Furthermore, tubes and sampling lines limit the patient's ability to move and breathing masks impede speaking, eating and drinking.

Regardless of its inconvenience, capnography is a reliable method to monitor respiration. Due to its accuracy, capnography is currently regarded as the gold standard in respiratory rate measurement. Thus, it is no surprise that it is more accurate in measuring respiratory rate than IP [19]. Capnography is the natural choice of reference for respiration measurement, therefore it was used when evaluating the accuracy of other methods in this thesis.

2.2.2 Impedance pneumography

In sub-acute care setting, impedance pneumography is the most common non-invasive method of monitoring respiration. IP, also known as impedance plethysmography, can be conducted simultaneously with ECG using the same electrodes. Measuring impedance with a cableless, wearable equipment frees the patient from being chained to a hospital bed or patient monitor. IP is a very attractive method for monitoring respiration in ambulatory setting, but the technique faces challenges related to unreliability caused by movement artefacts.

The IP measurement is based on the change in thoracic impedance caused by the changes in the volume ratio of blood, bone and tissue due to respiration [18]. During inspiration impedance increases, and decreases during expiration [18].

In IP, low-current ($<$100 μA), high-frequency (20-100 kHz) signal is passed through the chest using a pair of electrodes, and the change in voltage is measured by the same or another pair of electrodes. In bipolar measurement only two electrodes are used, while tetrapolar measurement requires two pairs of electrodes, one for feeding the current and another for measuring the voltage. [12, p. 107-113] Tetrapolar measurements have the benefit of ignoring the impedance between electrodes and skin, and focusing the measurement sensitivity field into the area of interest [20]. A medical imaging technique that uses 16 or 32 electrodes placed around the thorax to monitor lung function or reconstruct an image of the lungs from impedance measurements is an application of electrical impedance tomography (EIT).

The selection of the carrier frequency should be made knowing that frequencies below 10 kHz are associated with high electrode skin impedance and frequencies above 100 kHz are limited by radio frequency interference and coupling of the subject to ground. The signal-to-artefact ratio is better with higher frequencies. [21]

The amplitude of the high-frequency carrier signal is modulated by respiration: inspiration increases and expiration decreases the amplitude. The respiration waveform is acquired as the envelope of the modulated carrier signal by using a demodulator. [18] Some signal processing steps often conducted involve low pass filtering to remove instrumentation noise, and high pass filtering to remove drift and baseline fluctuations [20].

When the alternating current (I) is known and voltage (U) is measured, the electrical impedance can be calculated analogous to Ohm's law.

$$Z = \frac{U}{I} \tag{9}$$

Equation 9 shows that impedance is directly proportional to voltage. Therefore, an increase in impedance yields an increase in the amplitude of the enveloped signal as observed during measurements.

Impedance describes the degree to which a circuit, or the thoracic cavity as is the case with IP, resists current flow. Impedance is not a scalar but a complex value, which means that in addition to magnitude, impedance has a phase. The real part of impedance equals electrical resistance and the imaginary part reactance which has both inductive and capacitive components. With direct current (DC), impedance

equals resistance, since DC has zero phase, and Equation 9 converts to Ohm's law. Impedance has the same unit as resistance, Ohm (Ω).

Electricity tends to take the path of least resistance. In the case of IP this means that most of the current flows through blood and muscle which have lower resistance than bone or air in the lungs. When IP is measured simultaneously with ECG using standard clinical electrode placement, such as the Einthoven Leads I or II (between right arm and left arm, or right arm and left leg, respectively), the main path of the current passing through the chest is quite superficial, which may impair estimation of TV, as only little current runs through the lung tissue. In fact, the IP signal results from chest wall distortions due to lung expansion and not from the volume of air in the lungs per se. [12, p.109-121]

On the other hand, there is evidence that the amplitude of impedance respiration waveform correlates with TV at least qualitatively [22, 23]. Figure 5 is an example of recorded and filtered impedance pneumogram over five breaths of decreasing TV. It is obvious that the decrease in the amplitude of the impedance oscillation is related to decreased TV.

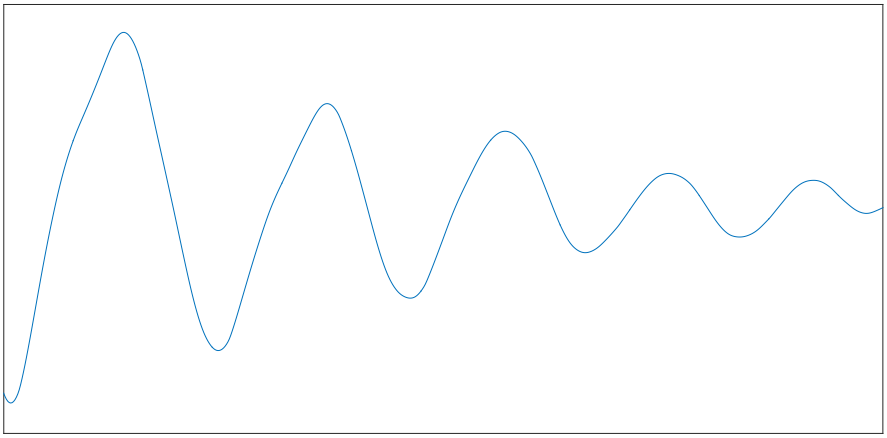

Figure 5: Impedance pneumogram over five breaths of decreasing volume. Data band pass filtered by a 2nd order Butterworth filter with passband from 0.08 to 0.5 Hz, which equals RR of 4.8-30 brpm.

IP does not measure actual air flow to and from the lungs but rather the respiratory effort largely contributed by muscles [12, 24]. When a patient is breathing normally without moving, RR can be calculated with reasonable reliability from respiration waveform, but when the patient's airways are obstructed, IP may incorrectly interpret the patient's attempts to breathe as real breaths. Thus, detecting obstructive apnea with IP is a challenging endeavour, if the patient expresses strong breathing efforts.

The degree to which the amplitude of the IP signal correlates with TV is affected by electrode position. Due to convenience of the simultaneous recordings, IP is often measured using standard ECG electrode positions. However, ECG electrodes are placed to optimize the acquisition of the electrical signals originating from the heart,

but the same electrode locations are not optimal for IP. Inconsistent results about the optimal electrode configuration exist in the literature. Some references claim that anterior-posterior leads offer the best correlation to tidal volume [12], while others have proof that lateral configurations have higher correlation coefficients [25]. One quite popular approach is to place electrodes bilaterally on the mid-axillary line on the level of the xiphoid process and a third electrode on the shoulder [22] or lower abdomen [26]. A commercial monitoring solution measuring RR by IP with two electrodes placed on the sides performs well when compared against a capnograph [27]. IP can be conducted using traditional disposable electrodes but also with textile electrodes integrated into clothing [28, 29].

In tetrapolar IP, the maximum sensitivity is obtained when the drive and receive electrodes are placed over the same lung on different horizontal planes [30]. When conducting tetrapolar IP, the voltage measuring electrodes have been placed also on the arms [23]. Especially in the estimation of TV, a more caudal electrode placement may result in poor correlation, and modification to the electrode locations requires changes also to the calibration between respiration waveform and TV [22]. For example, median impedance-volume ratios can be used as calibration factors to transform impedance into volume [20].

In addition to lead configuration, IP is also sensitive to motion, because most of the current is expected to propagate through the muscles in the chest and back. Any motion, related to breathing or not, contributes to the impedance signal. [24] Furthermore, the beating of the heart superimposes oscillations on the impedance signal, which are considered noise when measuring IP. The change in impedance is associated with the movement of the heart and pulsating blood flow, not with the electrical activity of the heart. [12] The amplitude of the cardiovascular artefact correlates with stroke volume, a fact exploited in impedance cardiography to assess cardiac output [31].

Cardiogenic artefacts impede the detection of real breaths from the respiration waveform especially when the frequency bands of RR and heart rate overlap, or when breathing is so shallow that cardiovascular artefacts may erroneously be interpreted as breaths. This may occur if bradycardia coincides with apneic event, and the amplitude of the cardiogenic oscillations increase resembling shallow breathing [18]. Cardiovascular artefacts can be suppressed by means of electrode configuration, ECG comparison, or using signal processing and different filtering methods, such as simple low pass filtering or non-linear Savitzky-Golay smoothing [20], or more advanced ensemble averaging techniques [32].

A change in the patient position requires modification of the calibration used to calculate TV from respiration waveform because the amplitude changes [22, 20]. Body position affects the way chest and abdomen expand during ventilation: while resting in horizontal position, the abdomen is relaxed and expands during inspiration. In a standing or seated position the abdominal muscle tone is increased, reducing the abdominal expansion. In an upright or seated position the expansion is primarily in the chest, and in supine position the expansion is principally in the abdomen. [12, p.114-115]

The size of a patient affects IP measurements. Although the base impedance

is approximately 500 Ω regardless of body size [12, p. 111-113], the change in impedance during respiration is greater in the smallest animals as observed in a study investigating the measurement of TV by IP in rats [26]. The estimation of TV also seemed to be worse for patients with higher body mass index [25].

Figure 6 demonstrates four periods of simulated apnea of about 20 seconds each. Periods 1 and 2 refer to simulated apnea by holding breath after inspiration and expiration, respectively. Periods 3 and 4 refer to simulated obstructed apnea where during similar breath holding the volunteer continued to make breathing movements. It can be seen that the waveform is relatively flat during simple breath holding, but during simulated obstructed apnea the impedance oscillates at almost the same amplitude as normal breaths. The chest movements during the last two periods are registered as breaths by the algorithm that uses threshold-based breath detection. The algorithm places small pointed peaks at detected breaths, and these can be seen also in the upper graph of Figure 6. In this example IP is able to detect simulated central apnea, since the cardiogenic artefacts are of low amplitude, but on another volunteer the amplitude of the cardiogenic artefact was so high that each heart beat was registered as a breath. Due to these false positive breaths, a patient monitor may in fact alarm for high RR instead of apnea during similar conditions.

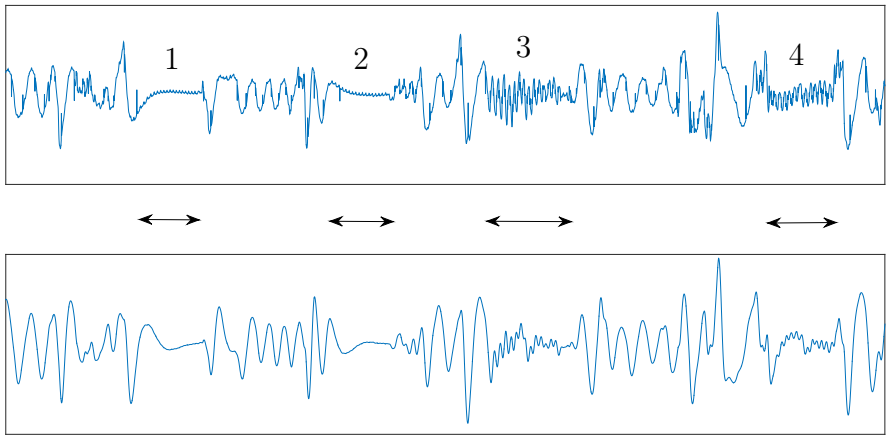

Figure 6: Impedance pneumogram over four periods of simulated apnea. Top: unfiltered data. Bottom: data band pass filtered by a 2nd order Butterworth filter with passband from 0.08 to 0.5 Hz, which equals RR of 4.8-30 brpm.

2.2.3 Respiratory inductive plethysmography

Respiratory inductive plethysmography (RIP) is a non-invasive technique well suited to continuously monitor respiratory rate in the ambulatory patient population. RIP measures changes in the circumference of the chest and abdomen with two respiratory belts. The RIP transducers contain sinusoidally arranged wire coils and the basis of the measurement is that a change in the length of the wires alters the self-inductance

of the wires resulting in a change in the oscillatory frequency. After demodulating and amplifying the frequency changes, the resulting signals are proportional to lung volume changes, but not able to measure absolute volumes. [18] Figure 7 presents these signals over five respiratory cycles.

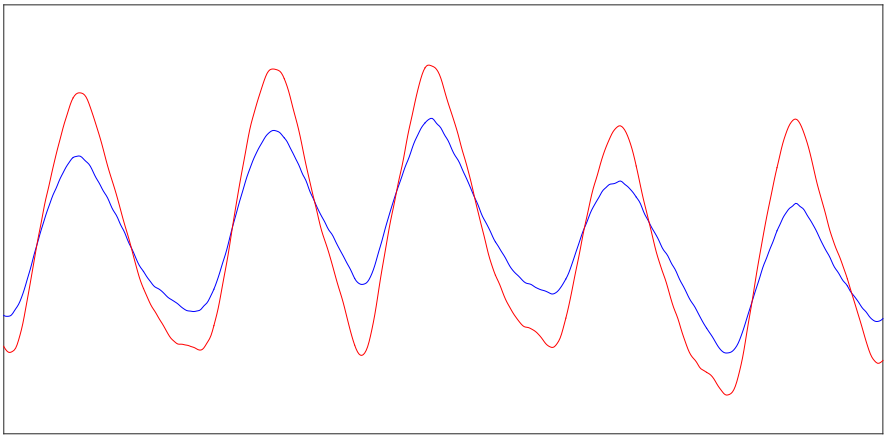

Figure 7: Respiratory waveform over five breathing cycles measured with respiratory inductive plethysmography. Signal from chest sensor (blue) has smaller amplitude than signals from the sensor around the abdomen (red).

2.2.4 Other methods

Expired air differs from room air in a way that can be exploited to measure respiration. Capnography takes advantage of the fact that expired air contains more CO_2 than room air, but it is also often warmer, which can be measured using a thermistor [33] or a pyroelectric sensor [34, 35]. Similarly, moisture in the exhaled air can be detected using a micro-condensation sensor [36] or a fibre-optic sensor [37].

Air moving in and out of the lungs can be measured indirectly by microphones recording the sounds of flowing air in the airway. Acoustic respiration measurement already exists as a commercial application, where the acoustic sensor is attached to the patient's neck. Respiratory rate monitored by acoustic method is shown to correlate well with capnography on several occasions: on adult [38] as well as pediatric [39] post-surgical patients, during treadmill tests [40], and during intravenous sedation of disabled individuals undergoing dental procedures [41], to name a few. Many of these studies also conclude that acoustic monitoring is better tolerated by patients compared to capnography with a breathing mask or nasal cannula. In one of these studies, the main error source for acoustic method has been identified as snoring [41]. Compared with capnography, acoustic and impedance methods have similar bias but acoustic method may be more precise in terms of limits of agreement [42].

Radio-Frequency (RF) applications present another approach to measure respiratory rate. Radar applications may be premised on Doppler's effect [43] or attenuation

of RF waves propagating through the thorax due to the changes in the dielectric properties of the lungs between inspiration and expiration [44]. The latter approach resembles IP in the sense that respiration alters the attenuation of RF waves passing through the thorax as it alters the impedance resisting current flow through the thorax.

Respiration can be monitored indirectly also by detecting respiratory movements with accelerometry or ballistography [45]. Next section discusses accelerometers in more detail.

2.3 Detecting movements with accelerometers

Accelerometers measure acceleration in one, two or three dimension depending on the design of the sensor. Instead of measuring acceleration as the rate of change in velocity accelerometers measure acceleration relative to free-fall, in g-forces. This means that even though the acceleration of an accelerometer (ACC) lying still on a table is zero, the reading would be 1 g. The value of standard acceleration due to gravity, g, is 9.81 m/s^2.

Triaxial accelerometers measure proper acceleration in three orthogonal directions: x, y, and z. The standard gravity can be thought of as a vector in the coordinate system of the accelerometer, where each acceleration component is the projection of that vector on the corresponding axis. Thus, the magnitude of acceleration, a, can be calculated as the magnitude of a vector in three dimensional space:

$$a = \sqrt{a_x^2 + a_y^2 + a_z^2} \tag{10}$$

When the sensor is not moving the equation 10 yields $a = g$. All three components are relatively stable when the sensor is immovable.

Both movement and changes in the orientation of the ACC are seen as variation in the readings. Movements create transient changes in the three components, whereas a change in orientation is seen as a change in the magnitude or level of the components. In the absence of fast movements, the greatest magnitude is measured in the direction of the axis that is most parallel to the vertical direction, i.e. the direction of gravity. This fact enables the determination of the orientation of the ACC. For example, the ACC in Figure 8 would measure zero in y and z directions and 1 g in x direction, if the sensor is held with x axis straight upwards.

Figure 9 shows the acceleration measured in x, y, and z directions during different activities. It can be deduced, that the orientation of the measurement sensor has been x axis up since acceleration in the x direction oscillates around 1 g. The oscillations are of greatest magnitude in the x direction during walking and jumping.

Accelerometers attached to the torso can detect respiratory motion and provide input for RR measurement. An acceleration derived respiration (ADR) waveform can be constructed from triaxial acceleration data by calculating angular changes [46] or by constructing an acceleration vector combining the three components [47]. However, general motion induces oscillations of greater magnitude than respiratory motion, which impedes the detection of breaths in the presence of other motion. Furthermore, ADR based on angular rates is sensitive to changes in the orientation of the ACC.

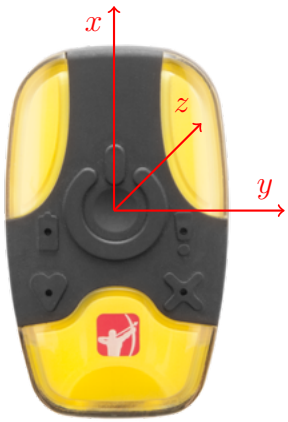

Figure 8: Coordinate system axes of a triaxial accelerometer. The z axis points away from the reader. (Faros 360, Mega Electronics).

Thus, the RR measurements are discontinuous, interrupted by patient changing position. When ADR is based on acceleration vector the estimation of RR might be continuous but require static conditions, which render the method feasible only during sleep or rest. Again, rejecting the periods containing more movements can increase the overall reliability while discontinuing the RR calculation. The advantage of this approach is that the estimation of RR is quite reliable when given, and the obvious drawback is that the estimation is not always available.

Other ADR methods are also able to provide continuous estimation of RR based on, for example, adaptive band-pass filtering based on energy expenditure and power spectral analysis [48]. These methods often prove more reliable with higher intensity movements, such as walking and running, compared to low intensity movements,

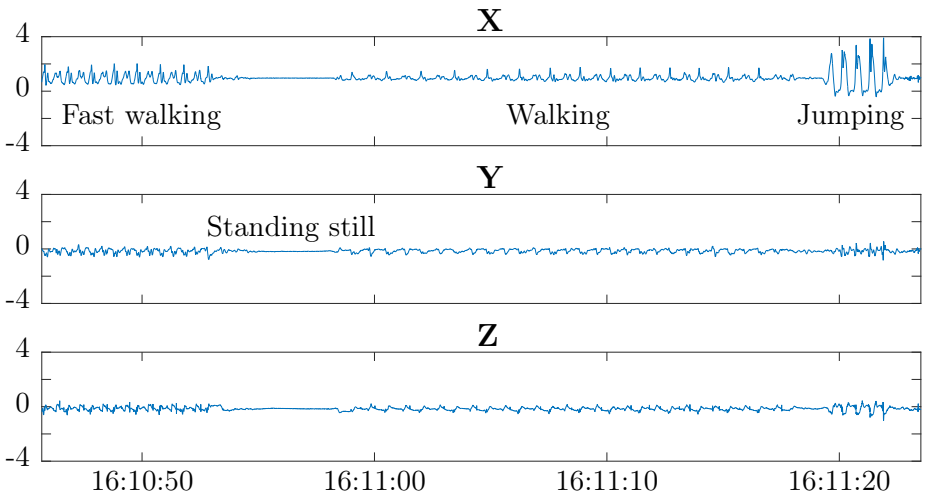

Figure 9: Output of triaxial accelerometer recorded during exercise. The unit in y axis is g.

such as slow walking or sitting with minor movements that are more characteristic of patients on general hospital wards.

Accelerometers alone can be used to derive respiration waveform but they have also been combined with other data sources in order to calculate RR. One example is to use ADR in combination with EDR to measure high breathing rates that cannot be measured by EDR due to cardiac aliasing [49]. This kind of data fusion can be realized by weighted averaging with quality metrics to weight the most reliable method over others. Such a quality metric can be derived from multiple features, such as the coefficient of variation of peak-to-peak amplitudes, the mean peak-to-peak amplitude, the coefficient of variation of the time between consecutive minima, and the ratio of the number of true maxima and minima to all local extrema. [49] Another example is to couple ADR with EDR or RIP based on energy expenditure calculated from ACC data [50]. Energy expenditure can provide an estimate of the level of movement intensity, i.e. whether the patient is sitting, walking, or running. This knowledge can be used to decide the combination of methods to use or weighting of derived RR values.

2.4 Deriving respiration from other physiological measurements

Respiration modulates cardiac function in a way that is observable through two common non-invasive measurements: ECG and pulse oximetry. This section describes how respiration modulates the associated waveforms of the two measurements and how respiration information can be extracted from these signals. Figure 10 illustrates the process of acquiring respiratory rate from impedance, ECG and PPG waveforms. After a respiratory signal has been derived from another waveform, it can be passed on to the same or very similar algorithm that calculates RR from impedance waveform. In theory, any physiological measurement that contains respiratory modulation could be used to derive respiration signal. ECG and pulse oximetry are selected for this

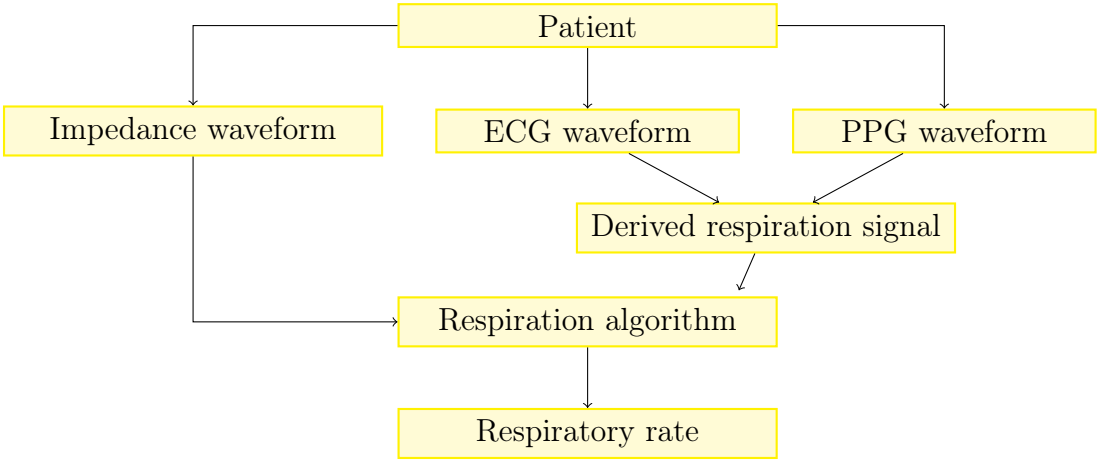

Figure 10: The process of acquiring respiratory rate from impedance and derived methods.

thesis because they provide non-invasive and easily available measurements also in the general ward environment.

2.4.1 Electrocardiography

The electrocardiogram represents the electrical activity of the heart. ECG is often measured with 3, 5 or 10 electrodes that are able to measure 1, 3 and 8 independent leads, respectively. The standard 12-lead ECG electrode placement is depicted in Figure 11. The four limb leads consist of right arm (RA), left arm (LA), right leg (RL), and left leg (LL) electrodes. Only RA, LA, and LL electrodes are used to measure ECG; the RL electrode is used as a grounding point. Lead I is measured between the arm electrodes, lead II between right arm and left leg, and lead III between left arm and left leg. The chest leads V1-V6 are measured with respect to Wilson's central terminal which is the average potential over the limb leads and represents the electrical potential of the heart. When using the 5-electrode configuration only one chest lead is measured in addition to the limb leads.

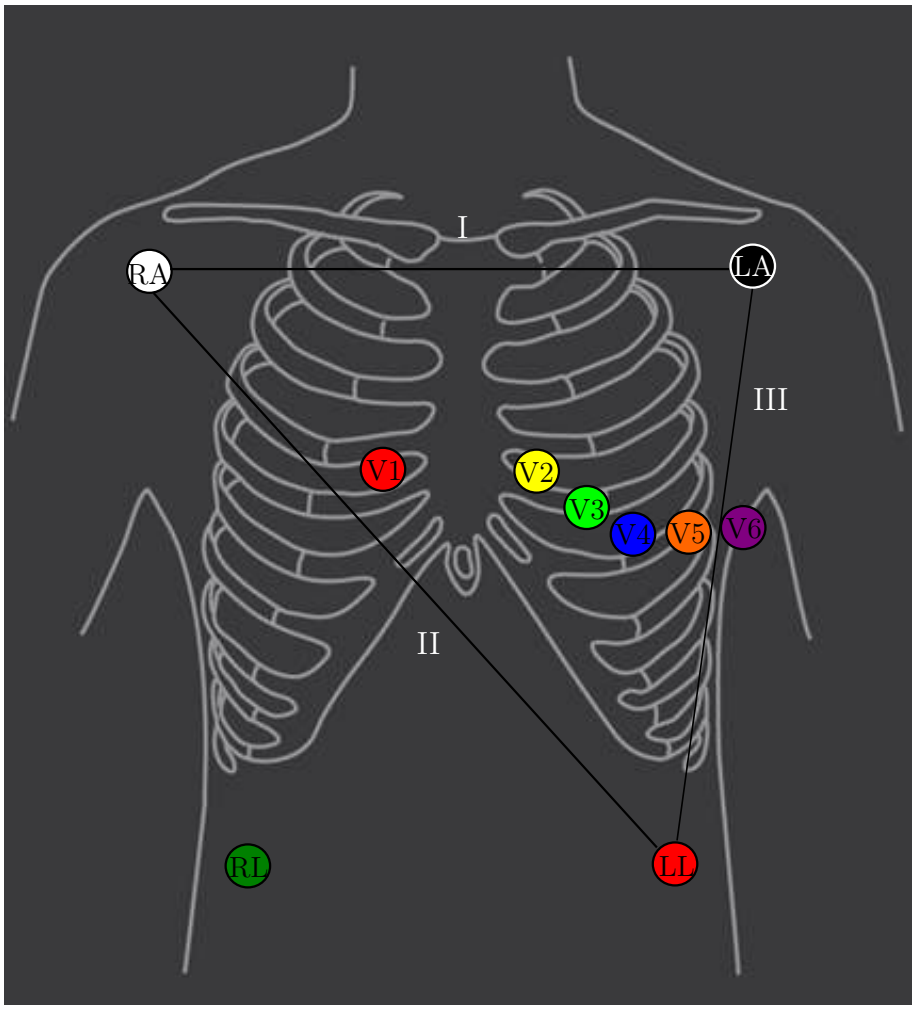

Figure 11: The standard 12-lead ECG electrode placement.

A normal ECG is presented in Figure 12. The ECG of one cardiac cycle includes the P-wave, QRS-complex, consisting of Q-, R- and S-waves, and T-wave. The P-wave is caused by the depolarization of the atria while the QRS-complex results from the depolarization of the ventricles and the T-wave from their repolarization [16, p. 112-114]. Atrial repolarization occurs during ventricular depolarization and is hidden by the QRS-complex. Heart rate can be calculated from the time between successive R-waves, i.e. the R-R interval.

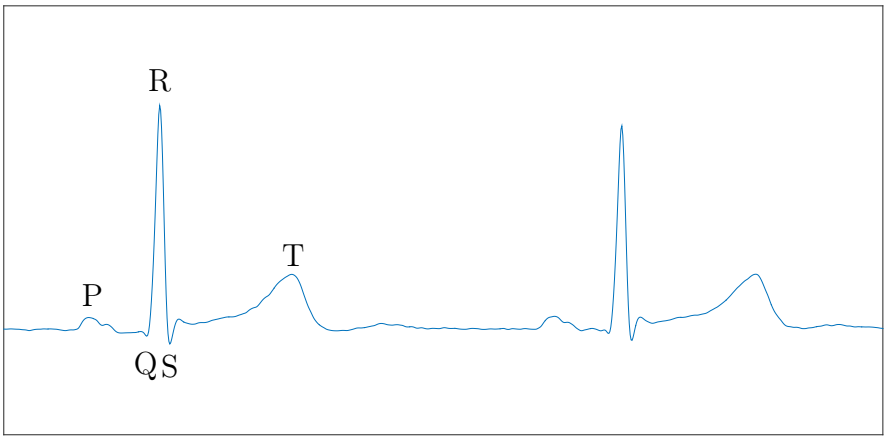

Figure 12: Electrocardiogram over two complete cardiac cycles. Data low pass filtered by a 2nd order Butterworth filter with cut-off frequency at 30 Hz to remove noise.

Respiration modulates the electrocardiogram by three different ways. First, the relative position of the electrodes and heart changes due to the movement of the rib cage and the respiratory muscles. The axis of the cardiac vector rotates during breathing because the position and orientation of the heart in the thoracic cavity varies between inspiration and expiration due to the expansion of the lungs and the movement of the diaphragm [51]. Second, the changes in the thoracic impedance caused by respiration also affect the ECG [52]. Respiration modulates the amplitude and morphology of the ECG, best seen in the QRS-complexes, through these changes. The amplitude of R-wave differs between leads as each lead only measures the electrical activity in the direction of the lead.

In addition to the amplitude modulation, respiration affects cardiac rhythm. The baroreceptors in the main and peripheral arteries control heart rate and respond to the pressure changes caused by respiration. It can be easily seen on the ECG that the heart beats faster during inspiration and slower during expiration. This phenomenon, referred to as the respiratory sinus arrhythmia (RSA), is best seen on healthy young people and diminishes with old age. RSA causes the R-R interval to decrease during inspiration and to increase during expiration. RSA may be suppressed by pacemakers or medication affecting cardiac rhythm. Naturally, the premise of this method breaks down in the presence of ventricular arrhythmias. [53] Figure 13 illustrates the effect of RSA and amplitude modulation on the ECG.

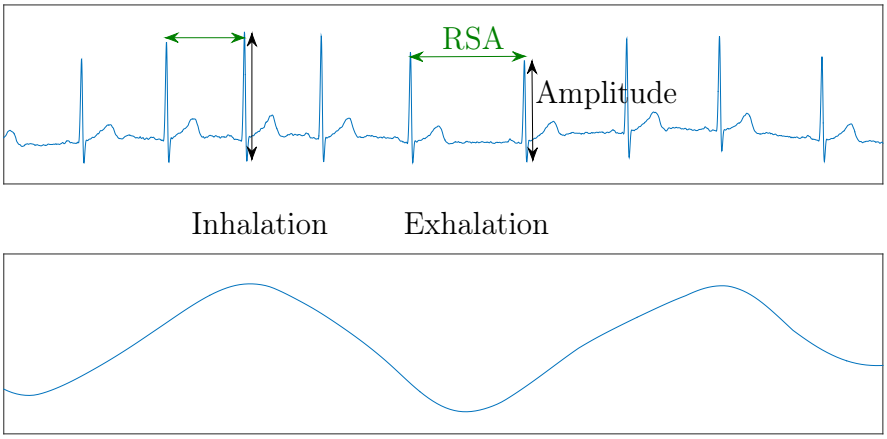

Figure 13: Respiration modulates heart rate and the amplitude of the R-wave as seen in these simultaneously recorded ECG (top) and impedance respiration waveforms (bottom). The R-R interval (green) is shorter and the R-amplitude (black) greater during inspiration than during expiration.

In 1985, Moody et al. [54] first introduced ECG-derived respiration. They derived respiration signal from two orthogonal ECG leads by calculating the angle of the mean cardiac electrical axis with respect to a lead axis using a method based on QRS areas. The areas under each QRS-complex were calculated over a fixed window determined by the interval from the PQ junction to the J-point after subtracting the baseline. With a fixed window width, QRS area is proportional to the amplitude of the R-wave and therefore also to the projection of the cardiac vector on the measuring lead. As the leads are assumed orthogonal, the arctangent of the ratio of the QRS areas of both leads yields the angle of the cardiac vector in relation to one of the leads. [54] The angle changes depending on the phase of respiration as described above. A signal constructed from the angle values by interpolation thus closely resembles respiration signal.

Zhao et al. combined the same technique with spectral analysis to obtain respiratory frequency from ECG with good correlation. They noted that the EDR is 180 degrees out of phase with respiration measured with IP, but this does not affect the spectra which was obtained by fast Fourier transform (FFT). [51]

The accuracy of the EDR method obviously depends on the width of the window in which the QRS area is calculated. Caggiano and Reisman compared three different methods to determine the window width where the width was either fixed or measured for each QRS-complex and the timing of windows on both leads was synchronized or not. Based on the average cross-correlation results they suggested that the timing of the windows for both leads should be synchronized. [55]

Travaglini et al. modified and applied the QRS area method to eight-lead ECG [52], but later different single-lead methods have gained success. Dobrev and Daskalov developed a device for infant heart rate and apnea monitoring which measured the R-

wave peak-to-peak amplitude using only two electrodes [56]. In R amplitude method, the respiration signal is derived from ECG by filtering the cubic spline interpolation of the R amplitude values [53]. EDR based on R amplitude has become one of the most popular methods due to its simplicity and relatively good correlation. R amplitude method has been evaluated against QRS area method and found to perform slightly but not significantly better [57]. Methods based on R amplitude variation can be divided into two categories: some use baseline wander noise removal [58] while others measure the peak-to-peak amplitude without any baseline correction [53]. According to Helfenbein at al. an advantage of the amplitude method is that it also correlates with TV [53].

Another popular approach is to analyse heart rate variability (HRV) and detect the component that is caused by RSA and thus matches the respiratory frequency. The HR spectrum contains also a low-frequency component below 0.05 Hz associated with temperature or vasomotor control, and a frequency band ranging from 0.06 to 0.15 Hz correlated with blood pressure control, the so called (Traube-Hering-)Mayer wave [51]. Normal respiratory frequencies are mainly above the Mayer wave but lower respiratory rates overlap with it, making it more difficult to separate the two.

In the RSA method, R-R intervals or heart rates are simply calculated and used to produce the respiration signal by cubic spline interpolation. According to Cysarz et al. both EDR based on R amplitude and RSA methods provide reasonable estimates of RR in younger subjects, but amplitude-based EDR should be preferred in the elderly [59]. Generally, algorithms based on R amplitude seems to perform slightly better than those based on RSA [60]. However, RSA methods produce signals with peaks at end-inspiration and troughs at end-expiration which conveniently matches the points of maximum and minimum TV [53].

EDR methods depending on QRS detection have the advantage of being fairly resistant to muscle artefacts as the R-wave can quite reliably be detected in the presence of noise. Even though these methods showed correlation to TV, they are unable to detect obstructive apnea. Another disadvantage of these EDR methods is that the signal is sampled at heart rate and depends on the accuracy of cubic spline interpolation to create the signal morphology. Thus, the signal may be under-sampled in the presence of bradycardia or tachypnea. [53] According to the Nyquist-Shannon theorem a signal should be sampled at a frequency of at least twice that of the highest frequency present in the signal or otherwise the signal cannot be perfectly reconstructed [61]. In the case of EDR, this means that only respiratory rates less than half of heart rate can be measured, a limitation known as cardiac aliasing.

Computationally more intensive and mathematically more complex methods exist alongside the simple R amplitude and RSA techniques. Bailón et al. introduced a method that utilizes least-squares alignment of three-dimensional QRS vectorcardiogram loops [62]. Langley et al. applied principal component analysis (PCA) for analysing the beat-to-beat changes in ECG morphology, and found that the variation in QRS-complexes correlates better with respiration than the changes in P- or T-waves. In terms of correlation and coherence, the single-lead PCA method was also found superior to the R amplitude and significantly better than the RSA method. [60] Widjaja et al. generalized the single-lead PCA method further by taking

into account possible non-linearities in the data by using a kernel function to map the data into a higher dimensional space where PCA was applied. The kernel PCA outperforms both PCA and R amplitude methods with statistical significance in correlation and coherence coefficients. [63] Tiinanen et al. also adapted linear PCA and independent component analysis (ICA) for deriving respiration from single-lead ECG with further improved results. Simultaneously they demonstrated that spline smoothing and resampling combined with bandpass filtering (2nd order Butterworth, passband 0.08-0.5 Hz) improved the performance of all EDR methods used in the article, including both advanced decomposition techniques and simple R amplitude method. [64]

Computationally less intensive alternatives to the methods previously mentioned are more attractive for real time applications. Labate et al. compared empirical mode decomposition (EMD) and wavelet analysis as EDR methods and found that EMD recovered the shape of the respiratory signal better than wavelet decomposition. EMD comprises an iterative subtraction of the average of the upper and lower envelope taken from the original signal [65]. Sharma et al. used simple homomorphic filtering which includes a non-linear mapping to a different domain, where the filtering is performed, followed by discrete Fourier transform. This method based on homomorphic filtering performs significantly better than the R amplitude method and similarly as the PCA, but is computationally less expensive. [66]

In a battery-powered device, the selection of underlying computation methods is strongly driven by the requirements of power consumption. The accuracy of calculations would have to improve significantly to outweigh the computational cost in order to select a more computationally expensive method as the base of an ambulatory application.

2.4.2 Pulse oximetry

Pulse oximetry is the standard of care for monitoring arterial oxygen saturation. The pulse oximeter emits light at two different wavelengths, i.e. red and infra-red, through the skin and measures the intensity of transmitted light. The sensor is often attached to a finger or an ear lobe, where the transmission of light occurs easily.

The absorption characteristics of hemoglobin depend on the amount of oxygen carried by the molecule. Oxygenated hemoglobin appears bright red while deoxygenated hemoglobin is dark blue. Oxygenated hemoglobin allows more red light to pass through than deoxygenated blood. Therefore, the two species can be differentiated. The wavelength of the infra-red light is selected so that approximately the same amount of light is transmitted through both oxygenated and deoxygenated blood. Thus, SpO_2 can be calculated from the ratio of red to infra-red transmission intensity. [12, p. 79-81]

The measured photoplethysmographic waveform has a pulsating appearance as demonstrated in Figure 14. Hence, the pulse rate can easily be calculated from the PPG waveform. The pulsating AC-component of the PPG waveform is caused by the time-varying absorption and scatter effects of the arterial blood. Venous blood does not pulsate and thus only affects the static DC-component or the baseline of the

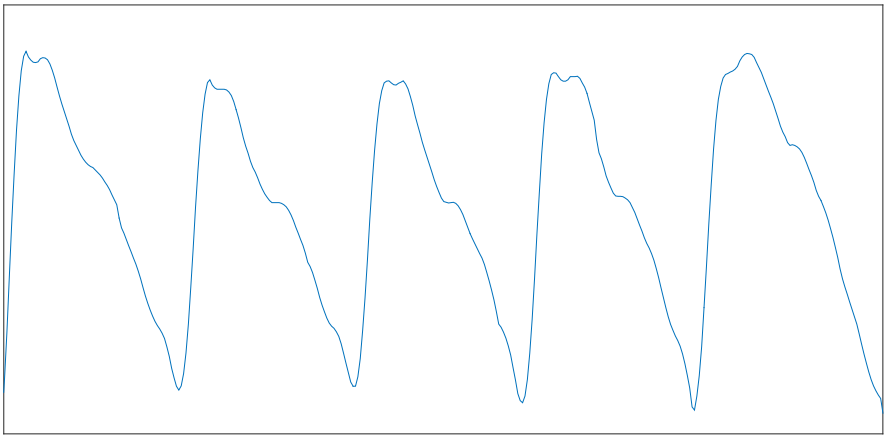

Figure 14: Typical shape of the photoplethysmographic pulse waveform.

PPG waveform among other tissues present in the measurement site, such as skin and bone. This distinction allows the differentiation between arterial and venous blood.

In addition to SpO_2 and pulse rate, the PPG waveform carries information about other functions, including respiration. Respiration modulates PPG waveform in three different ways as illustrated in Figure 15. Respiration modulates the amplitude and pulse width of the PPG but also the baseline. Methods aiming to derive respiration from PPG naturally track one or more of these modulated features.

The amplitudes of the PPG pulses are modulated by respiration because the

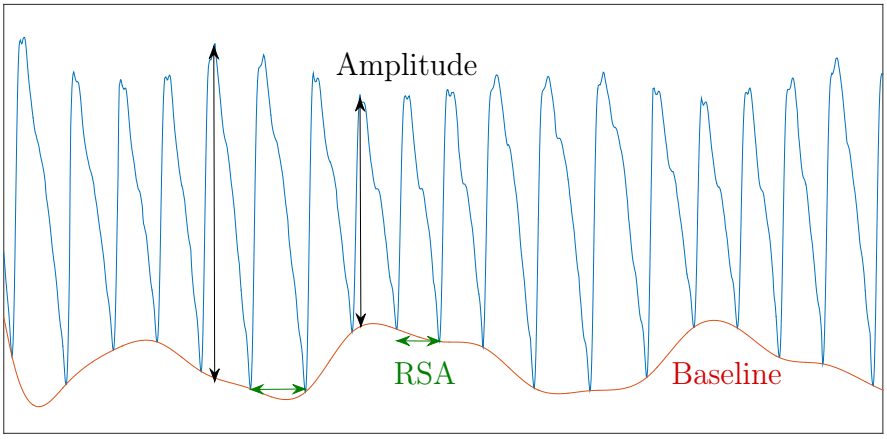

Figure 15: Respiration modulates PPG waveform in three different ways. Baseline modulation (red), amplitude modulation (black) and RSA (green) are all related to respiration.

stroke volume of the heart changes during respiratory cycle. During inspiration the pulse amplitude is lower than during expiration, since the left ventricular stroke volume is decreased and less blood is pumped into the site of measurement. [67, 68]

The baseline modulation stems from the changes in venous return in response to changes in intrathoracic pressure during respiratory cycle. During inspiration, the baseline rises as the venous bed is drained due to the decrease in intrathoracic pressure and causally also central venous pressure increasing venous return. During expiration, the baseline falls as the venous bed fills due to the decrease in venous return. [67, 68]

The pulse rate modulation or RSA was already introduced in connection with ECG and the same effect can be seen in PPG waveform as pulse width variability. RSA causes the pulses of the PPG waveform to widen during expiration and to narrow during inspiration.

Since the PPG morphology differs from ECG, methods based on RSA use different approaches. Lázaro et al. derived respiration from PPG pulse width instead of calculating the interval between successive pulses [69]. However, RSA may not be manifested in the PPG of all patients. Similarly amplitude or baseline modulation may not be expressed, as it varies from patient to patient which modulations can be clearly observed from the PPG. Thus, Addison et al. have developed an algorithm for calculating pulse oximetry derived respiration. Their algorithm uses advanced signal processing capabilities, such as continuous wavelet transform coupled with weighted averaging and logical decision making processes. [67, 68]

Dash et al. have compared wavelet and complex demodulation techniques of ECG, PPG and piezoelectric pulse transducer (PZO) signals to derive respiration. They tested these time-frequency methods for accuracy and repeatability with results indicating that PPG-based methods outperformed approaches based on both ECG and PZO. [70] However, this result cannot be generalized as only wavelet and complex demodulation were compared.

Empirical mode decomposition can be conducted on PPG as well as on ECG [71]. EMD performs iterative subtraction of the mean of the upper and lower envelope from the original signals, breaking the signal down into a finite number of individual components called intrinsic mode functions (IMF). IMFs are characterized by two conditions: the number of extrema and the number of zero crossings must be equal or differ at most by one, and at any point the mean of the upper and lower envelope of the IMF is zero, in other words the upper and the lower envelope are symmetrical with respect to zero. [72] Unlike wavelet analysis, EMD extracts basis functions from the original signal, obliterating the need for pre-defined mother wavelet [71].

Once IMFs have been produced the next step is to evaluate which of the IMFs represents respiration. EMD is often coupled with spectral analysis and the right IMF is selected by the main frequency peak. However, it can be speculated that the main frequency of more than one IMF may fall into the respiratory frequency range. If the patient is breathing abnormally fast or slow, the method might choose a value that is closer to the normal respiratory rate.

Figure 16 shows the first three IMFs of the PPG waveform. It can be seen that the higher the ordinal number the lower the frequencies left in the IMF. The first

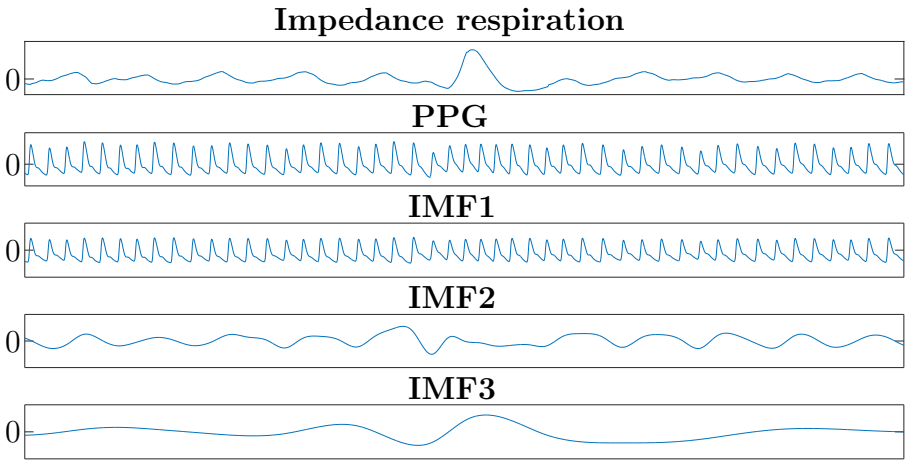

Figure 16: PPG and the first three IMFs as decomposed by EMD. Here the second IMF contains respiratory frequencies.

IMF resembles the original signal, but fulfils the two conditions of IMFs. In fact, the main frequency of the first IMF corresponds to heart rate. The second IMF seems to match well with impedance respiration, while the third IMF obviously contains lower frequencies.

2.5 Motion artefacts

Motion artefacts (MA) are recognized as the greatest challenge of wearable biomedical sensors and systems [73]. All physiological measurements contain noise and artefacts due to motion or other factors interfering with the target function. In case of IP, these artefacts impede the detection of breaths from the impedance waveform. Similarly with derived respiration methods, disturbances in the original waveforms cause oscillations in the derived signal not related to respiration. The susceptibility of IP to motion artefacts has been compared with RIP as well as piezoresistive and piezoelectric respiration belts [74]. During cycling and running, piezoelectric pneumography was found statistically most robust against movement artefacts, but IP was least corrupted by MA during walking, which makes IP more applicable to general hospital ward environment.

Motion artefacts in IP have been studied in the past and many MA reduction techniques regarding the hardware and measurement design have been identified. First, using higher carrier frequency improves the signal-to-artefact ratio (SAR) [21]. Second, electrode properties that minimize movement artefacts include strong adhesion, good physical stability, low baseline impedance, large effective area, and large total area [75, 76, 77]. Large adhesive area around electrode provides mechanical stability against MA arising from skin stretching during movement. Third, movement artefacts can be reduced by electrode placement. In bipolar IP, anterior-posterior electrode placement where one electrode is placed on the sternum at the level of

the second intercostal space and the other in the opposite position on the back has been claimed to maximize SAR [75]. Movement artefacts were successfully rejected by another electrode placement using six electrodes, two on midsternal line, two on vertebral line, and two bilaterally over the Latissimus dorci muscles on the upper back [78]. Electrodes in the middle of sternum or back are considered to be less affected by arm movements since they are as far away as possible from both arms and over rigid bony structures. However, IP is often conducted simultaneously with ECG through the same electrodes and the electrode placement is optimized for ECG.

In addition to measurement equipment design, signal processing can be used to improve reliability. There are two possible approaches: detect the artefact and remove it, or detect the artefact and indicate low signal credibility. It depends on the application which approach is the most appropriate. Artefact removal requires a reference signal that correlates to the target function or to the artefact. These signal processing methods can also rely on single or multiple data sources. An example of multi-parameter approach in MA cancellation is using accelerometers as the reference signal source. ACC data have been used as reference signal in adaptive motion artefact reduction with RIP and ECG. With RIP and high intensity movement the motion artefact cancellation works well, but not for medium or low intensity movements. For ECG, ACC is a poor source of reference signal because the motion artefact in ECG is induced by stretching the epidermis of the skin which is not recorded in the acceleration signal. [79]

Using two different carrier frequencies and adaptive filtering can reduce motion artefacts in IP. This method is based on the finding that the amplitude ratio between two signals measured with different frequencies differed between normal breathing and movement. Due to this, a signal strongly related to movement only can be constructed to be used as reference signal in adaptive filtering for motion artefact reduction. [80]

3 Materials and methods

The feasibility study reported in this thesis consists of four segments presented in Figure 17. Preliminary data collection, algorithm development, and algorithm evaluation were conducted by the author of this thesis, whereas the primary data collection was carried out elsewhere.

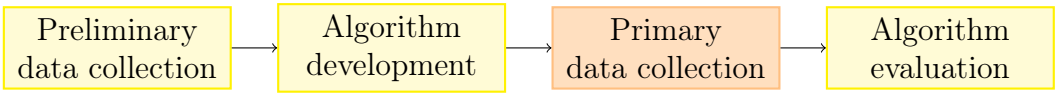

Figure 17: Process diagram of this thesis work.

3.1 Data collection

Data was collected on two separate settings. The preliminary data collection was performed in Helsinki with two volunteers, and the data was used in algorithm development. The primary data used in further development and analysis was collected from 10 volunteers by VTT in Tampere.

3.1.1 Measurement equipment

For the preliminary data collection, five ECG electrodes were placed on the volunteer's torso: the limb leads on right and left shoulder and on right and left lower rib cage and the chest lead on V1 position, i.e. 4th intercostal space at right border of sternum. The volunteer was connected to the patient monitor (CARESCAPE Monitor B450, GE Healthcare) equipped with a Patient Data Module via ECG cables and a SpO2 reusable sensor (LNCS DCI, Masimo Corporation). The volunteer breathed through a mask which was connected to the gas module (CARESCAPE Respiratory Module, GE Healthcare) via a gas sampling line. An accelerometer (Faros 360, Mega Electronics) was also taped onto the chest of the volunteer. The patient monitor was connected to a laptop computer (Latitude E6430, Dell) that collected the signals with S/5 Collect software (GE Healthcare). The following waveforms were collected during the test: ECG, PPG, impedance respiration, CO_2, flow, airway pressure, and the 3D-acceleration. ECG was sampled at 500 Hz, acceleration at 400 Hz, PPG at 100 Hz, and impedance respiration, CO_2, flow and airway pressure at 25 Hz.

For the primary data collection, the measuring equipment was transported to Tampere where two experimenters were required to conduct the measurements. The measurement set-up differed by the number of various sensors, but most of the additional equipment and acquired signals were not utilized in this work. Raw PPG waveforms were collected using three different sensors, active cables, and another collection software. All three pulse oximetry sensors were placed on the left hand and circulated between index, middle, and ring finger. The PPG signals used in the analysis were collected from the same type of sensor.

Additional accelerometers (ActiGraph) were attached to volunteer's wrist, upper arm, and ankle. Two more accelerometers (Faros 360, Mega Electronics) were

attached to both sides of the chest. The accelerometer in the middle of the chest also collected single-lead ECG which was not utilized here. The sampling rate of the accelerometer was dropped to 100 Hz because of the simultaneous ECG measurement.

Due to the high number of required sensors and electrodes and the complexity of the set-up, the placement of the five primary ECG electrodes slightly varied between patients. The limb leads were placed close to the standard positions, but the chest lead was positioned around the area approximately 10 cm below the standard V4 position. This non-standard chest lead is later referred to as the lead C. Non-invasive blood pressure measurements were conducted intermittently by a measurement cuff, but the data was not processed in the analysis at all.

The changes applied to the respiratory monitoring are as follows: Instead of the breathing mask, nasal cannula was used to measure CO_2. Airway pressure and flow were unavailable using this equipment. Also, two respiration belts (Embla, Natus Medical Incorporated) based on RIP technology were added into the set-up and placed around the thorax and abdomen. The signals acquired from the RIP sensors were processed in the same manner as the impedance respiration waveform for comparison purposes.

3.1.2 Test protocol

The test protocol for preliminary data collection varied between recordings. The tests contained different actions performed in supine, half sitting, sitting and standing positions, including free, fast, slow, deep, and shallow breathing, simulated episodes of both central and obstructed apnea, abdominal and chest breathing, couching, talking, eating, drinking and moving. Central apnea was simulated by simply holding breath for 20 seconds and obstructed apnea was simulated by trying to continue breathing motion during breath holding. Naturally, the breathing mask had to be removed during eating and drinking. For this reason, one of the test recordings is missing the reference for respiration. Another test had to be discontinued because breathing through the mask started to feel too heavy. More precise descriptions of test protocols are provided in Appendix A.

The primary data collection was conducted using a fixed protocol comprising of movements typical for general ward patients, such as sitting on a bed, walking, and climbing stairs. The full protocol can be found in Appendix A. During measurements the experimenter was required to carry all measurement equipment to enable the volunteer to move freely. The following information was recorded: subject identification code, date of birth, gender, weight, height, and dominant hand. Also, the placements of the three pulse oximetry sensors were recorded and varied between volunteers.

3.1.3 Volunteers

The primary data collection was conducted with 10 volunteers (50% male, all right-handed). The demographics of the volunteers are presented in Table 2. One volunteer had to be excluded from the analysis due to a failure to record data from the monitor,

including impedance and reference signals. Small gaps present in some recordings were considered acceptable.

Table 2: Volunteer demographics

	Age (years)	**Weight (kg)**	**Height (cm)**	**BMI (kg/m^2)**
Range	26-51	57-85	163-195	21.3-25.7
Average	36	70.7	177.1	22.9
SD	8.2	8.6	8.3	1.5

3.2 Algorithm development

The algorithms developed for this thesis consist of those calculating respiratory rate and deriving respiration signals from ECG and PPG. The universal algorithm developed for respiratory rate calculation from all derived respiration signals was also able to process impedance waveforms as it was independent of the scale of the input signal and defined a unique threshold for each signal.

3.2.1 Signal preprocessing

Figure 18 illustrates the signal preprocessing steps done by the author of this thesis after VTT had collected, synced and stored the primary data in files in European

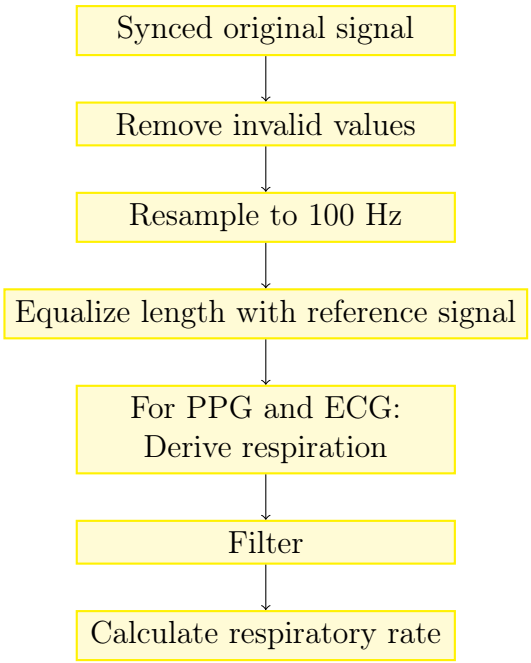

Figure 18: Block diagram of signal preprocessing steps before RR calculation.

Data Format. The processed physiological data consisted of PPG, CO_2, impedance respiration, inductance respiration (RIP) and ECG waveforms. ECG standard leads I, II, and III were used as well as a non-standard chest lead.

The physiological data and simultaneously recorded 3D acceleration data were loaded from files and processed in floating point format. Invalid values, i.e. values less than -32000, were replaced by NaN-values to be ignored in most calculations. All signals were resampled to 100 Hz and cut to the length of the reference signal, which was the CO_2 waveform. PPG was originally sampled at 100 Hz, so this had no effect on the extraction of the pulse oximetry derived respiration signals. ECG-derived respiration signals were extracted from the original waveform sampled at 500 Hz. All respiration signals were filtered by a 2nd order Butterworth filter with passband from 0.08 to 0.5 Hz prior to RR calculation. Impedance respiration signal was resampled when a function call to one of the already existing algorithms required it.

3.2.2 ECG-derived respiration methods

Derived respiration signals were extracted from single lead ECG data using two different methods: amplitude and RSA-based. A third approach that derived respiration by calculating the relationship between data from two separate ECG leads was also implemented. This method is here referred to as the cardiac angle method, as it aims to track the changes in cardiac angle during breathing. The amplitude and RSA modulations were discussed in Section 2.4.1.

Figure 19 illustrates the signal processing steps required for the EDR methods used in this thesis. Detecting QRS-complexes from the ECG is the first step of all

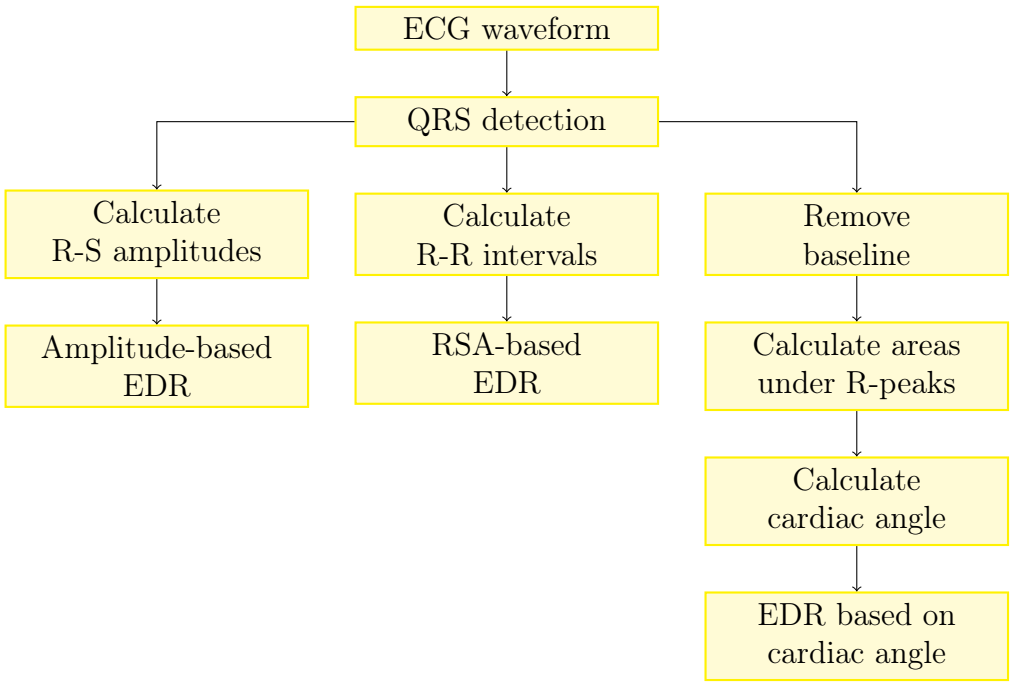

Figure 19: Signal processing steps required for EDR methods.

these EDR methods. QRS detection was conducted by using an already existing ECG-algorithm that provided approximations of R-peak locations. The exact locations were found by searching for the maximum values close to the approximate locations. Additionally, the locations of S-peaks required for amplitude method were defined as the minimum values no later than 100 ms after the corresponding R-peaks.

In amplitude-based method, the amplitude of the R-peak is calculated as the difference between R-peak and the corresponding S-peak. The derived respiration signal is then constructed by cubic spline interpolation of these values. The RSA-based method is otherwise similar but is based on the R-R intervals instead of R-S amplitudes.

The cardiac angle method used ECG data from two separate leads. After detecting the R-peaks, the baseline is removed from both signals by adapting the method from [58]. Baseline is constructed by cubic spline interpolation from mid-point values between R-peaks and subtracted from the original signal resulting in a flat waveform without baseline wander. The R-peaks are assumed to occur simultaneously in both signals.

After removing the baseline, areas under R-peaks are calculated in fixed windows of width 100 ms centred around the R-peak. The cardiac angle is calculated as

$$\alpha = \tan^{-1}\left(\frac{A_a}{A_b}\right), \tag{11}$$

where A_a and A_b are the areas under R-peak from two different ECG leads. The leads are here assumed to be orthogonal. Finally, the derived respiration signal is acquired by cubic spline interpolation of the cardiac angle values.

The derivation of all types of EDR signals depends strongly on the performance of QRS-detection and cubic spline interpolation. ECG waveform is only sampled at R-peaks, which means that the signal might be undersampled if QRS-complexes are missed during fast breathing. False R-peak detections also interfere with signal construction by adding false points before interpolation. Cubic spline interpolation is responsible for discovering the waveform shape of EDR signals.

3.2.3 Pulse oximetry derived respiration methods

Respiration signals were derived from PPG waveform using five different approaches: amplitude, baseline, RSA, pulse width, and EMD. These methods aim to extract respiratory modulation from the PPG waveform using different techniques. Amplitude, baseline and RSA modulations were discussed in Section 2.4.2.

Figure 20 presents the signal processing steps for amplitude, baseline, and RSA-based PDR methods. In the amplitude method, the respiration signal was calculated as the difference between the upper and the lower envelope of the PPG waveform. The envelopes were constructed with cubic spline interpolation from the local maxima and minima for the upper and lower envelope, respectively. The lower envelope was used as the respiration signal in the baseline method.

RSA and pulse width methods did not utilize the envelopes, but the local maxima and minima, respectively. Both methods calculated the intervals between successive

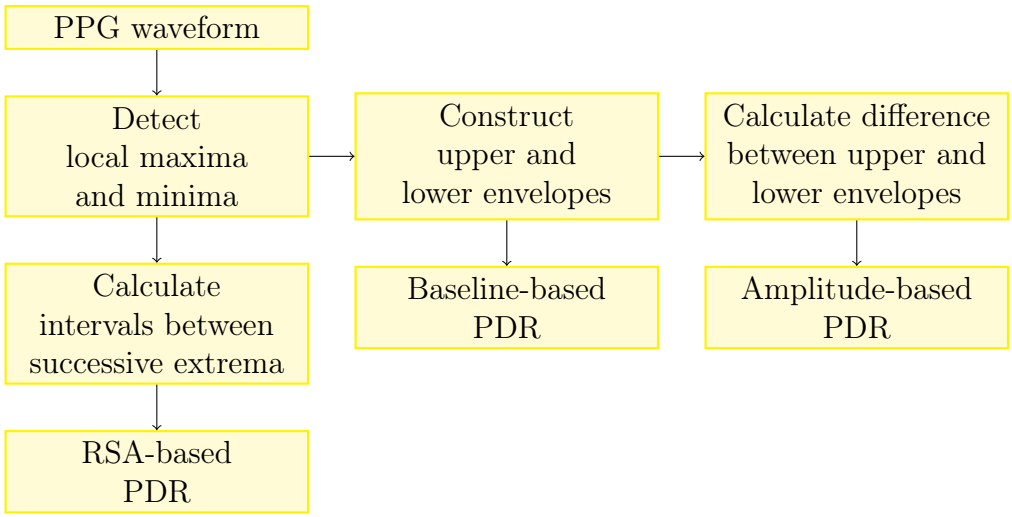

Figure 20: Signal processing steps required for PDR methods.

extrema and constructed a signal of these values by cubic spline interpolation. These derived respiration signals are quite similar with the difference that RSA calculates intervals between each pulse peak, whereas pulse width calculates the differences between the troughs of the pulses.

Figure 21 illustrates the steps of EMD process. The EMD algorithm is comprised of two loops: the outer loop keeps track of all IMFs and the inner loop calculates each IMF in a process referred to as sifting. Sifting begins by finding all local minima and maxima from the input signal, constructing upper and lower envelopes, and calculating their mean. This mean is then subtracted from the input signal to calculate a candidate IMF, h_{1k}, where k is the number of sifting iterations. To decide whether the candidate IMF should be accepted, it is compared to the previous result, $h_{1(k-1)}$, by calculating a standard deviation (SD) as

$$SD = \sum_{t=0}^{T} \left[\frac{|(h_{1(k-1)}(t) - h_{1k}(t))|^2}{h_{1(k-1)}^2(t)} \right]. \tag{12}$$

If the SD is more than a pre-defined value, the sifting process ends and the candidate is accepted as an IMF. If the SD is less than the pre-defined limit, the sifting process continues with the candidate as the new input signal. This work used a value of 0.3 as the SD limitation as suggested in [72].

Once the first IMF is extracted from the original signal, a residual is calculated by subtracting the IMF from the original signal. Then the next IMF is calculated by iterating on this residual. The whole process stops when the remaining residual contains less than two maxima or minima and the envelopes cannot be constructed. The original signal now equals the sum of all identified IMFs and the remaining residual.

Often EMD is followed by spectral analysis, but this work used a certain IMF as derived respiration signal in the same manner as the outputs of the other PDR-methods. Respiratory rates were calculated from each PDR-signal using the same

algorithm described in section 3.2.4.

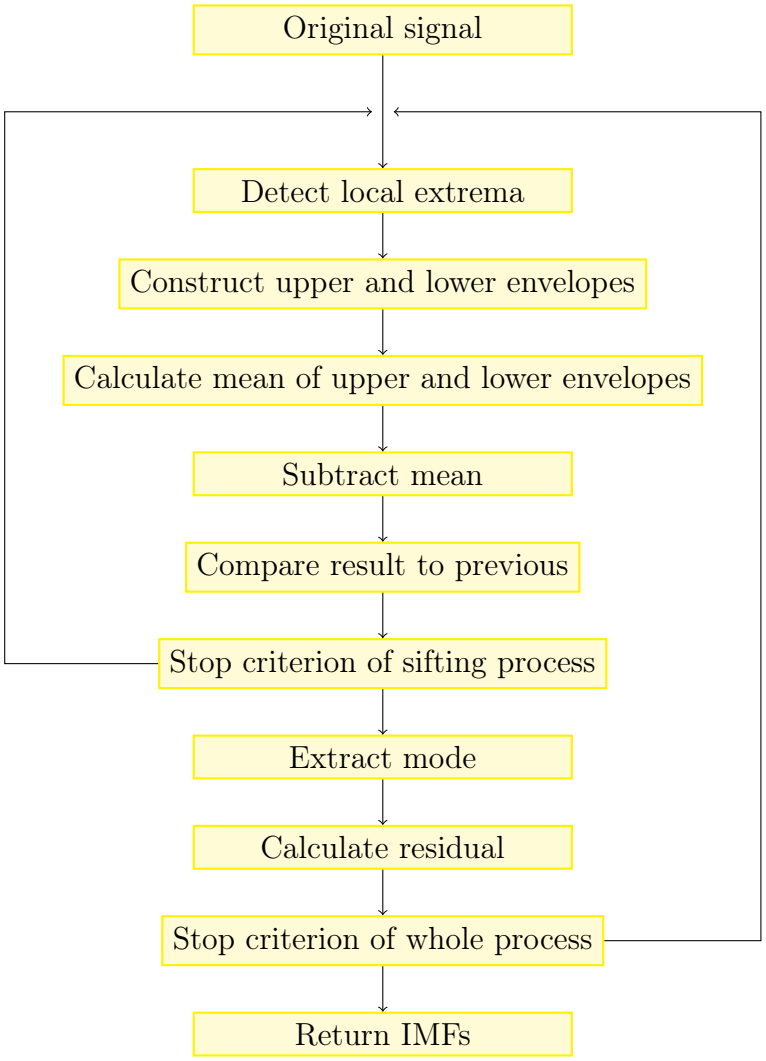

Figure 21: Block diagram of Empirical Mode Decomposition.

3.2.4 Respiratory rate calculation

The advanced counting method by Schäfer and Kratky [81] was slightly modified to create three respiratory rate calculation algorithm versions. The algorithm logic for the original advanced counting method can be described in five steps: (1) Filter the signal by a 10th order Butterworth band-pass filter (BPF) with passband of 0.1-0.5 Hz. (2) Find all local maxima and minima. (3) Take the absolute values of the vertical differences between subsequent local extrema and determine the third quartile $\hat{Q}_3$ of these to define a threshold value of $f\hat{Q}_3$, where $f = 0.3$ in case of respiration signal or $f = 0.1$ when using derived respiration signal based on RSA. (4) Remove all subsequent pairs of local extrema if the vertical difference between the maxima and minima is less than the defined threshold level. (5) Instantaneous

respiratory rate is the reciprocal length between subsequent remaining maxima, and average RR is their mean. [81]

In this work, the filtering is done as a preprocessing step before calculating RR. However, the filter design differs in terms of order and lower cut-off frequency; a 2nd order Butterworth BPF with passband of 0.08-0.5 Hz was used instead of 10th order with passband of 0.1-0.5 Hz. This decision was supported by a more recent publication [64].

The threshold factor f used to define the threshold value differs from those given above and ranges between 0.01 and 0.12. The factor was optimized for all methods and algorithm versions separately by maximizing reliability and accuracy, i.e. maximizing the time during which the error in calculated RR values was less than 20%, and minimizing the total mean absolute error.

The respiration detection part of the three algorithm versions varies. The first version obeys the logic of the original advanced counting method. The second version modifies the original logic by adding an additional requirement: in order to determine the oscillations originating from respiration all maxima were required to lie above zero and respectively all minima were required to lie below zero. In the third version, oscillations arising from breathing activity were required to be zero-centered, in other words the maxima were required to lie above $0.5 \times threshold$ and the minima below $-0.5 \times threshold$. Comparison of the performance of these three algorithm versions suggested that both versions 2 and 3 provided better results than the original algorithm, and the second algorithm version performed slightly better than the third. Thus, the second algorithm version was used in the analysis.

The algorithms express RR values in 1/min. In addition to breath-to-breath RR values the algorithm calculates display values. These values are calculated every 10 seconds by taking the weighted average over the last 30 seconds.

The algorithm developed here could be implemented as a real-time solution with some changes. The threshold could be determined during a learning phase in the beginning of the measurement or it could adapt to the amplitude of the signal as the measurement proceeds.

3.3 Algorithm evaluation

The algorithms developed for this thesis were evaluated together with four already existing impedance respiration algorithms. These algorithms are referred to here as Algorithm A, D, G, and R. The universal respiratory rate calculation algorithm developed for this thesis is named Algorithm U. This was used to calculate RR from the impedance as well as all derived respiration signals. The naming of all evaluated methods is clarified later in Table 3 in Section 4.

3.3.1 Performance measures

Capnography was used as the reference respiration measurement, and the reference RR from the CO_2 waveform was provided by another algorithm. The performance of all other methods was evaluated in relation to the reference. The error of each

measurement point was calculated as

$$\text{error} = RR_i - RR_{ref,i}. \tag{13}$$

Thus, a positive error means that the method overestimates the RR value. The error can also be expressed in percentage terms as

$$\text{error} = \frac{RR_i - RR_{ref,i}}{RR_{ref,i}} \times 100\%. \tag{14}$$

Here, an estimate is considered reliable if the error was less than 20%. Reliability of the methods is assessed by the fraction of time each method measures RR reliably, i.e. how often the error is less than 20%.

The bias of the methods was calculated as

$$\text{bias} = \frac{1}{N}\sum_{i=1}^{N} RR_i - RR_{ref,i}, \tag{15}$$

where N is the number of RR measurement samples, RR_i is the RR value measured by the method to be evaluated, and $RR_{ref,i}$ is the reference RR value. Essentially, bias equals mean error and describes the average difference between the measured and true RR. Positive bias means that the evaluated method tends to overestimate respiratory rate and bias close to zero indicates that the method does not have a systematic tendency to underestimate or overestimate RR. However, bias in not a measure of accuracy as too high and too low RR values cancel each other out. Thus, the accuracy of the methods was represented instead of mean error by mean absolute error calculated by

$$\text{accuracy} = \frac{1}{N}\sum_{i=1}^{N} |RR_i - RR_{ref,i}|. \tag{16}$$

Taking the absolute value of the error before calculating the average ensures that methods with smaller absolute errors have a value of accuracy closer to zero when compared to methods with larger absolute errors.

The precision of the methods is calculated as the standard deviation of the errors:

$$\text{precision} = \sqrt{\frac{1}{N-1}\sum_{i=1}^{N} (RR_i - RR_{ref,i} - bias)^2}. \tag{17}$$

The precision described how close the errors are to the mean error, or bias. A value close to zero means that the errors tend to be quite systematic, whereas a large value indicates that the errors are spread over a wider range of values and seem more random in nature. The bias and precision together can be used to characterize the distribution of errors. Assuming the errors are normally distributed, the bias would define the mid-point of the bell curve and precision would contribute to the height and width of the curve.

The overall correlation of measured RR values to reference measurement were evaluated by calculating Pearson correlation coefficients defined as

$$\rho(RR, RR_{ref}) = \frac{1}{N-1}\sum_{i=1}^{N} \left(\frac{\overline{RR_i - \mu_{RR}}}{\sigma_{RR}}\right)\left(\frac{RR_{ref,i} - \mu_{RR_{ref}}}{\sigma_{RR_{ref}}}\right), \tag{18}$$

where μ ans σ are the mean and standard deviation, respectively. Correlation coefficients close to one indicate good correlation between the evaluated method and the reference. Correlation coefficient is considered significant if the corresponding p-value is smaller than 0.01. Each activity was assumed independent while calculating the p-values. The number of independent samples was enough for all correlation coefficients calculated here to be considered significant.

3.3.2 Effect of different activities

In addition to the performance of the algorithms, the function during different activities was evaluated in terms of reliability and alarm performance. To assess the reliability of the methods during different activities, the percentage of time each method spend within error limit of 20% during each activity was calculated. Here the calculation of respiratory rate was regarded reliable if the error was less than the defined limit. The limit of 20% was considered reasonable and realistic but not too strict. Methods that most of time gave reliable results were considered robust.

The alarm performance of all methods during different activities was assessed by the amount of violations of alarm limits. The alarm limits were set at 5 and 30 breaths per minute for low and high RR alarms, respectively. Again, the percentage of time that the measured RR value was within these limits during each activity was calculated. The reliability and alarm performance criteria were tested both separately and simultaneously. Based on these assessments, activities that proved challenging for respiratory rate measurement were identified.

As a part of the activity evaluation also acceleration data was utilized. The relationship between level of acceleration and error was evaluated by calculating the prediction probability, P^K, described in [82] for each method separately. This was done in order to assess whether higher acceleration values were associated to increased errors during different activities.

4 Results

Table 3 summarises the names of all methods evaluated in this thesis. In addition to evaluating the performance of different algorithms and derived respiration methods the IP technology itself is also compared with RIP techniques as the Algorithm U is used to calculate respiratory rate from the signals provided by both technologies.

Table 3: Summary of all evaluated methods. ECG Lead X is always one of I, II, III, or C. Lead C refers to a non-standard chest lead.

Reference	
CO_2	RR based on CO_2 measurement
Impedance respiration algorithms	
Algorithm A	
Algorithm D	
Algorithm G	
Algorithm R	
Algorithm U	Universal algorithm developed for this thesis
EDR methods	
EDR Amp X	Amplitude-based EDR measured from ECG Lead X
EDR CA Y-X	EDR based on cardiac angle measured between ECG Leads Y and X, where Y is I, II, or C (nine combinations in total)
EDR RSA X	RSA-based EDR measured from ECG Lead X
PDR methods	
PDR Amplitude	Amplitude-based PDR
PDR Baseline	Baseline-based PDR
PDR EMD	PDR calculated by Empirical Mode Decomposition
PDR Pulse width	RSA-based PDR where pulse intervals are calculated from the troughs of the pulses
PDR RSA	RSA-based PDR where pulse intervals are calculated from the peaks of the pulses
RIP	
RIP Abdomen	Respiration signal from the belt around the abdomen
RIP Chest	Respiration signal from the belt around the chest
RIP	Respiration signal acquired as the sum of the signals from both belt sensors

4.1 Algorithm performance evaluation

Table 4 presents the averaged performance measures calculated for each method. Reliability is the percentage of time the method is able to give a reliable estimate of RR. Bias, accuracy, precision, and Pearson correlation coefficients, ρ, are calculated by Equations 15, 16, 17, and 18, respectively. These results are discussed in more detail in the following sections.

Table 4: Summary of averaged performance measures. All Pearson correlation coefficients are statistically significant ($p<0.01$).

	Reliability %	Bias 1/min	Accuracy 1/min	Precision 1/min	ρ
Algorithm A	60.9	-2.64	3.82	4.66	0.59
Algorithm D	59.1	-2.39	3.71	4.45	0.56
Algorithm G	36.8	-5.37	6.09	5.46	0.36
Algorithm R	52.8	3.44	6.29	10.48	0.58
Algorithm U	62.8	-0.75	4.30	6.58	0.56
EDR Amp I	51.4	-1.81	4.94	5.99	0.42
EDR Amp II	54.0	-1.24	4.64	5.82	0.36
EDR Amp III	53.7	-1.06	4.57	5.79	0.38
EDR Amp C	54.9	-1.38	4.49	5.72	0.36
EDR CA I-II	44.9	-0.59	5.48	6.43	0.37
EDR CA I-III	44.1	-0.46	5.79	6.98	0.33
EDR CA I-C	44.7	-0.40	5.53	6.44	0.39
EDR CA II-I	50.7	-1.81	4.87	5.96	0.34
EDR CA II-III	52.8	-1.27	4.70	5.87	0.35
EDR CA II-C	49.3	-0.34	5.04	5.99	0.34
EDR CA C-I	52.8	-1.91	4.69	5.82	0.35
EDR CA C-II	50.7	-1.70	4.83	5.85	0.36
EDR CA C-III	51.2	-1.11	4.74	5.86	0.38
EDR RSA I	36.0	-3.93	6.52	7.03	0.35
EDR RSA II	36.1	-5.38	6.52	6.13	0.38
EDR RSA III	35.0	-5.35	6.69	6.21	0.36
EDR RSA C	33.9	-6.00	6.71	5.72	0.38
PDR Amplitude	26.0	-7.17	8.91	7.29	0.21
PDR Baseline	25.4	-7.59	8.98	7.06	0.22
PDR EMD	30.4	-3.80	9.14	9.54	0.23
PDR Pulse width	29.1	-7.05	8.65	7.17	0.19
PDR RSA	26.7	-7.41	8.85	7.19	0.21
RIP Abdomen	67.3	-2.20	3.06	3.57	0.70
RIP Chest	62.5	-2.19	3.62	4.52	0.59
RIP	66.6	-2.22	3.09	3.61	0.69

4.1.1 Reliability

Reliability was evaluated as the percentage of time the measured RR had less than 20% error compared to the reference. The bar chart in Figure 22 shows the methods in order of decreasing reliability. It is obvious that the RIP measurement is slightly more reliable than the best impedance respiration algorithms which in turn are more reliable than any derived respiration method.

The universal Algorithm U outperforms other algorithms as it was optimized for the used dataset to be as reliable as possible. Algorithms A and D are more reliable than the Algorithm R which is of the same level with the best EDRs. Algorithm G is outperformed by most EDR methods based on amplitude and cardiac angle.

All EDR methods are more reliable than any PDR method. Among the EDR

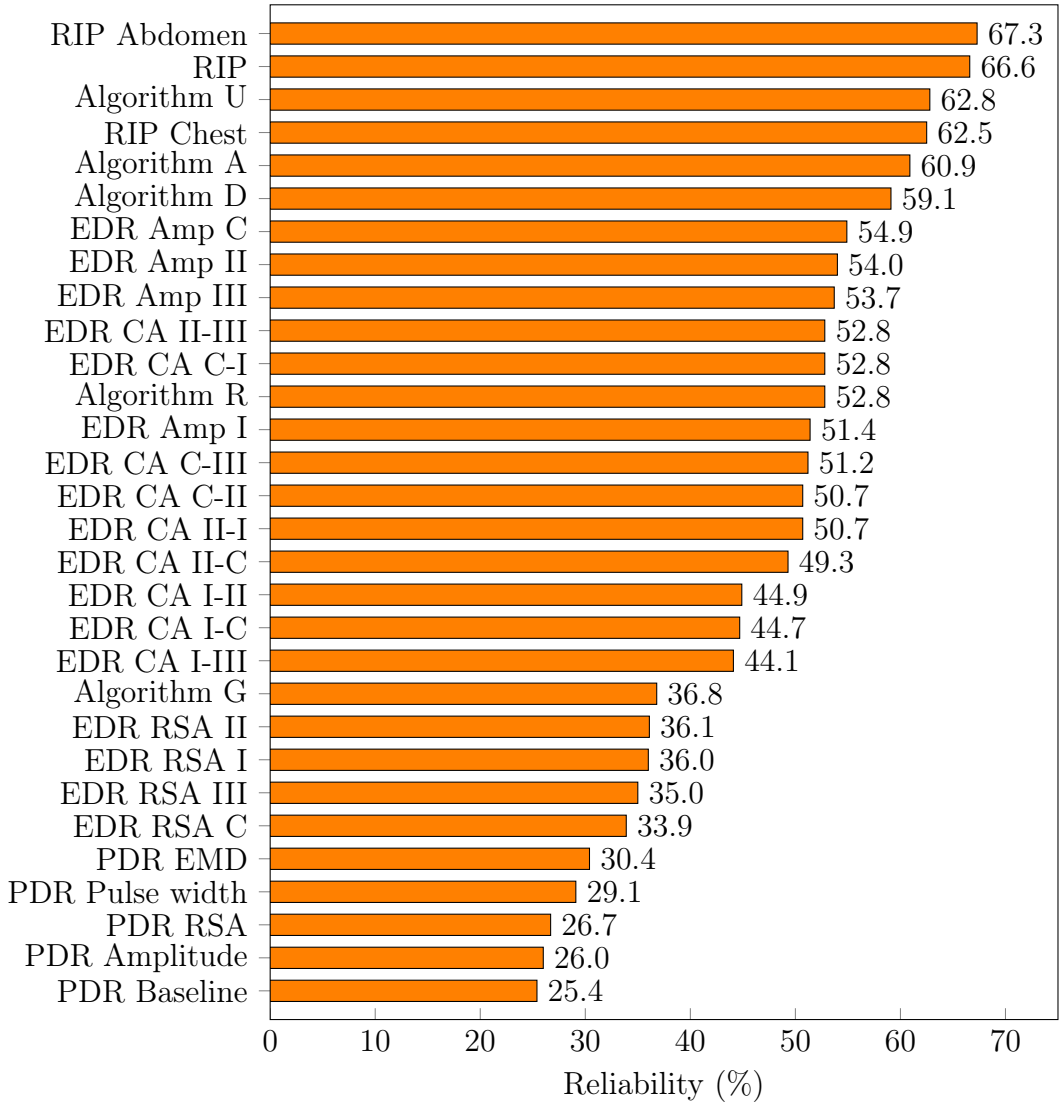

Figure 22: Reliabilities of all evaluated methods expressed as percentage of time the RR measurement was reliable, i.e. the error was less than 20%.

techniques, the amplitude-based methods are more reliable than majority of those based on cardiac angle. RSA-based methods are worse than the other two types of EDRs.

All PDR methods measured RR reliably less than 30% of time. PDR by EMD was more reliable than the RSA-based PDRs which in turn were more reliable than the amplitude and baseline-based PDR methods.

4.1.2 Bias

The bias equals average error. Figure 23 presents a bar chart of the biases of all evaluated methods. All methods except the Algorithm R tend to underestimate RR. The least biased methods consist of some cardiac angle based EDRs, Algorithm U, and amplitude-based EDRs. RIP is less biased than Algorithms D, A, and G. Algorithm

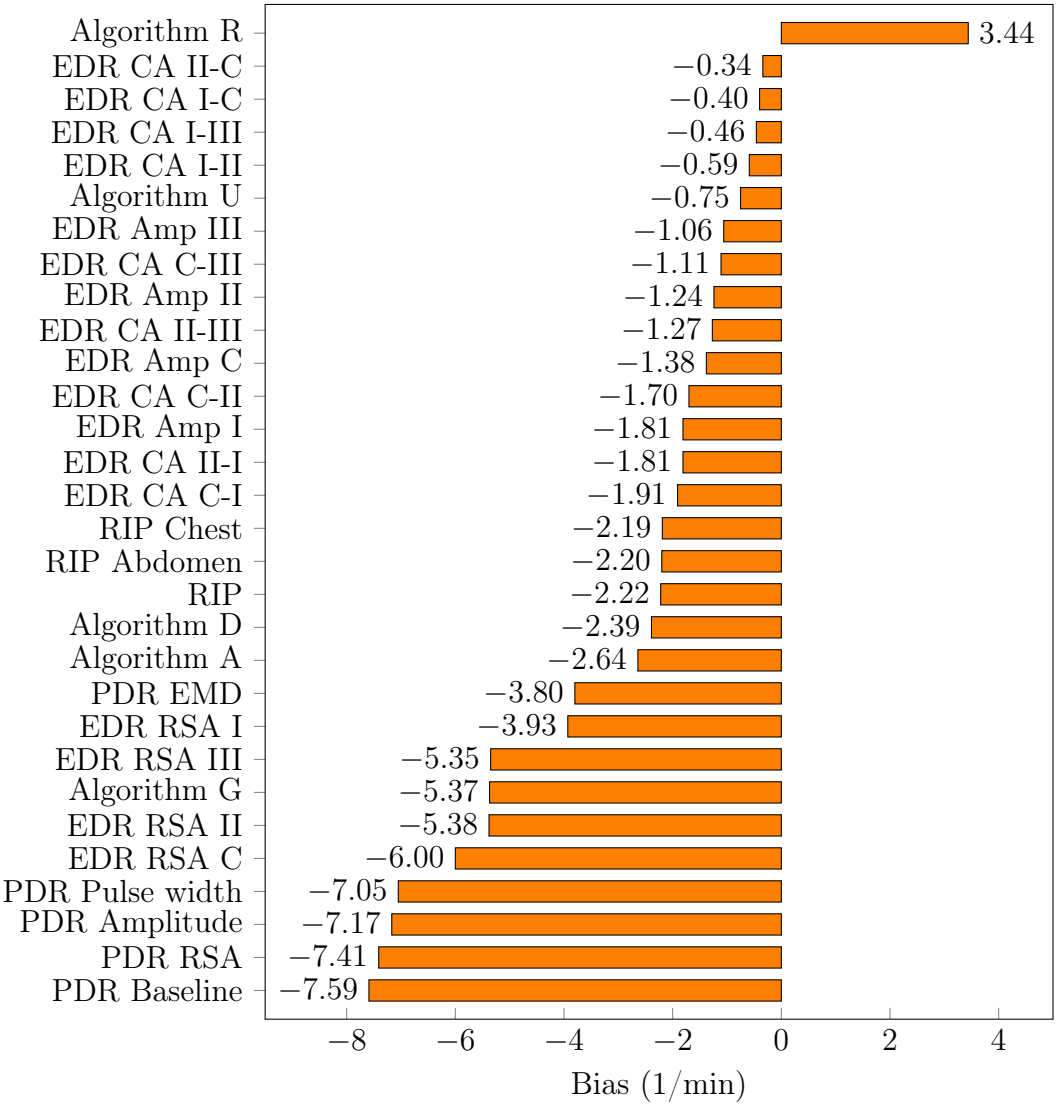

Figure 23: Biases of all evaluated methods.

R overestimates only slightly more than Algorithms D and A underestimate RR. PDR by EMD is less biased than all RSA-based EDR methods, but the other PDRs are the most biased methods.

4.1.3 Accuracy

Accuracy describes how close the measured RR is to the reference RR on average. All evaluated methods are put in order by decreasing accuracy in Figure 24. This order resembles that based on reliability with some changes. According to the acquired accuracies, RR values measured by RIP are on average closer to the reference RR than other methods. Algorithms D, A, and U are more accurate than any EDR or PDR method. Algorithms G and R are less accurate than the amplitude and cardiac angle based but more accurate than the RSA-based EDR methods. All PDR

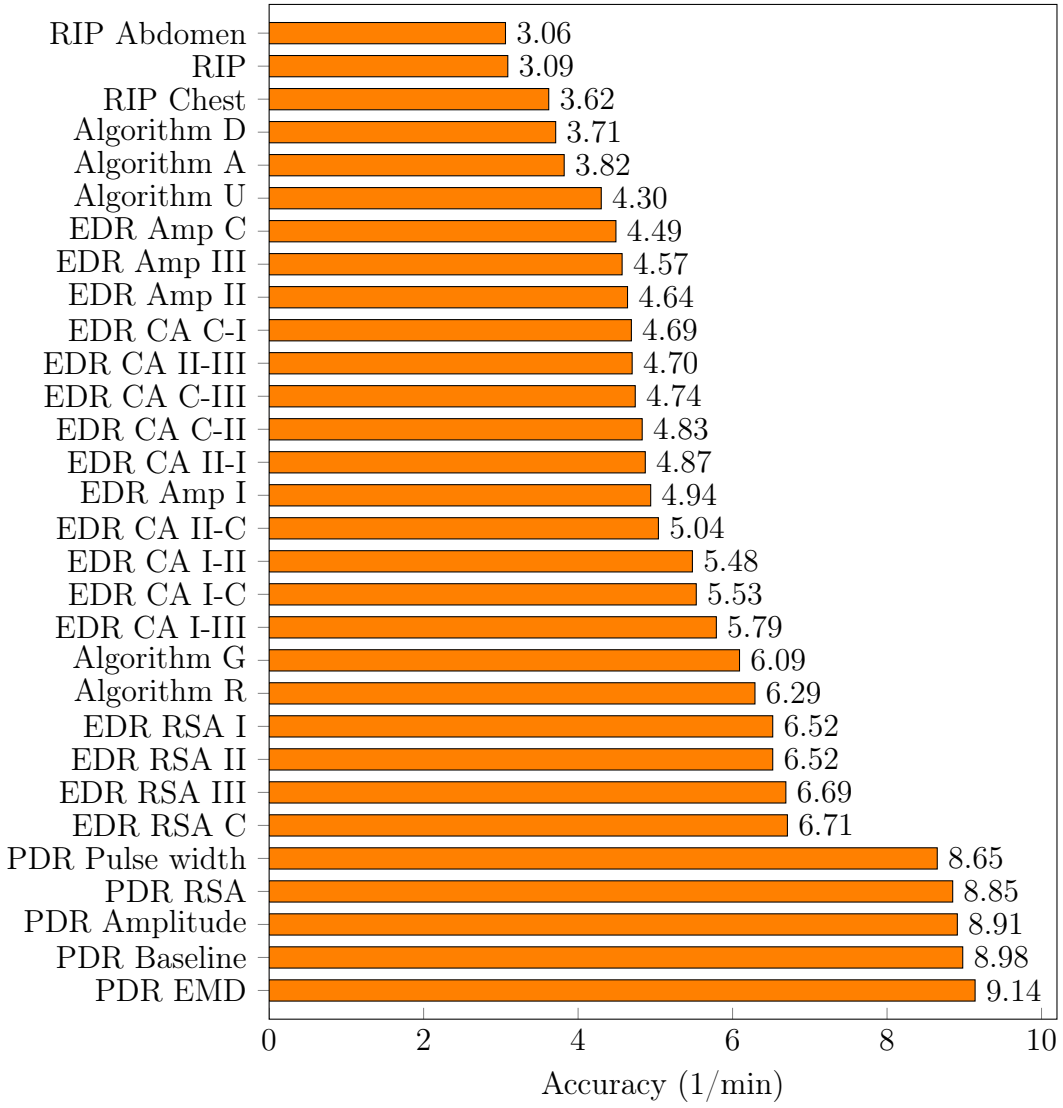

Figure 24: Accuracies of all evaluated methods.

methods are significantly less accurate than the other evaluated methods. Based on these results alone, it is quite clear that the feasibility of PDR methods evaluated here is poor.

4.1.4 Precision

Precision is the standard deviation of errors and describes the level of variation among errors. Figure 25 depicts the methods in order of increasing contingency of errors. RIP methods and also Algorithms D, A, and G seem to have more systematic error profile than the other methods. The precisions of EDR methods are quite close to each other, but again the order of amplitude, cardiac angle, and RSA-based EDRs seems to persist. The precision of Algorithm U is extraordinarily low as it is only two places above the poor PDR methods. However, even more surprising is the ranking

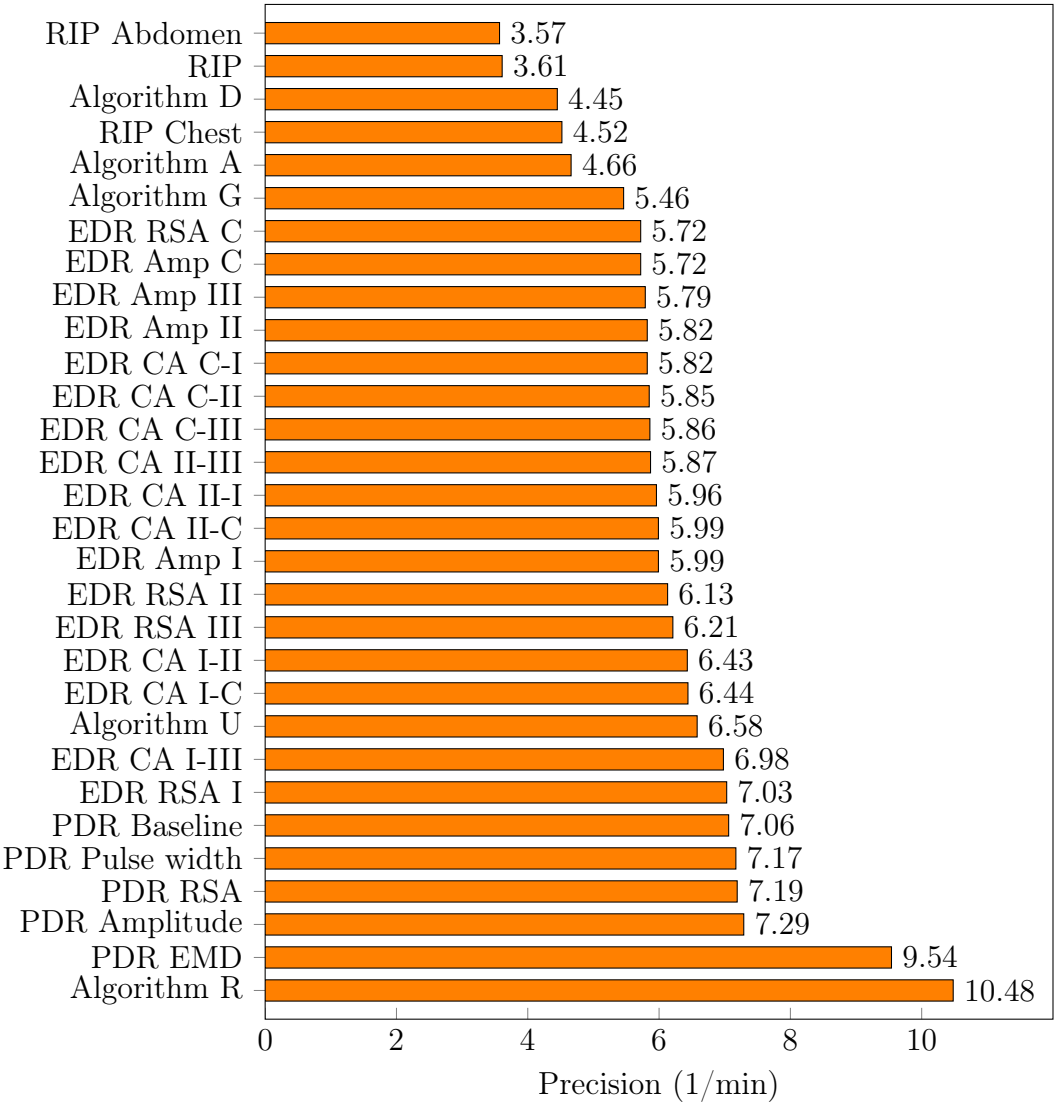

Figure 25: Precisions of all evaluated methods.

of Algorithm R in the bottom of the list.

4.1.5 Correlation

Correlation of measured RR values between each method and the reference describes how well the trend of measured RR follows that of the reference. Evaluated methods ordered by decreasing correlation are depicted in Figure 26. Again, the RIP methods outperform other methods. Algorithm A is closely followed by Algorithms R, D, and U. A clear drop in correlation coefficient values can be observed when comparing impedance algorithms and EDR methods. Another drop in correlation follows when moving from EDR to PDR methods.

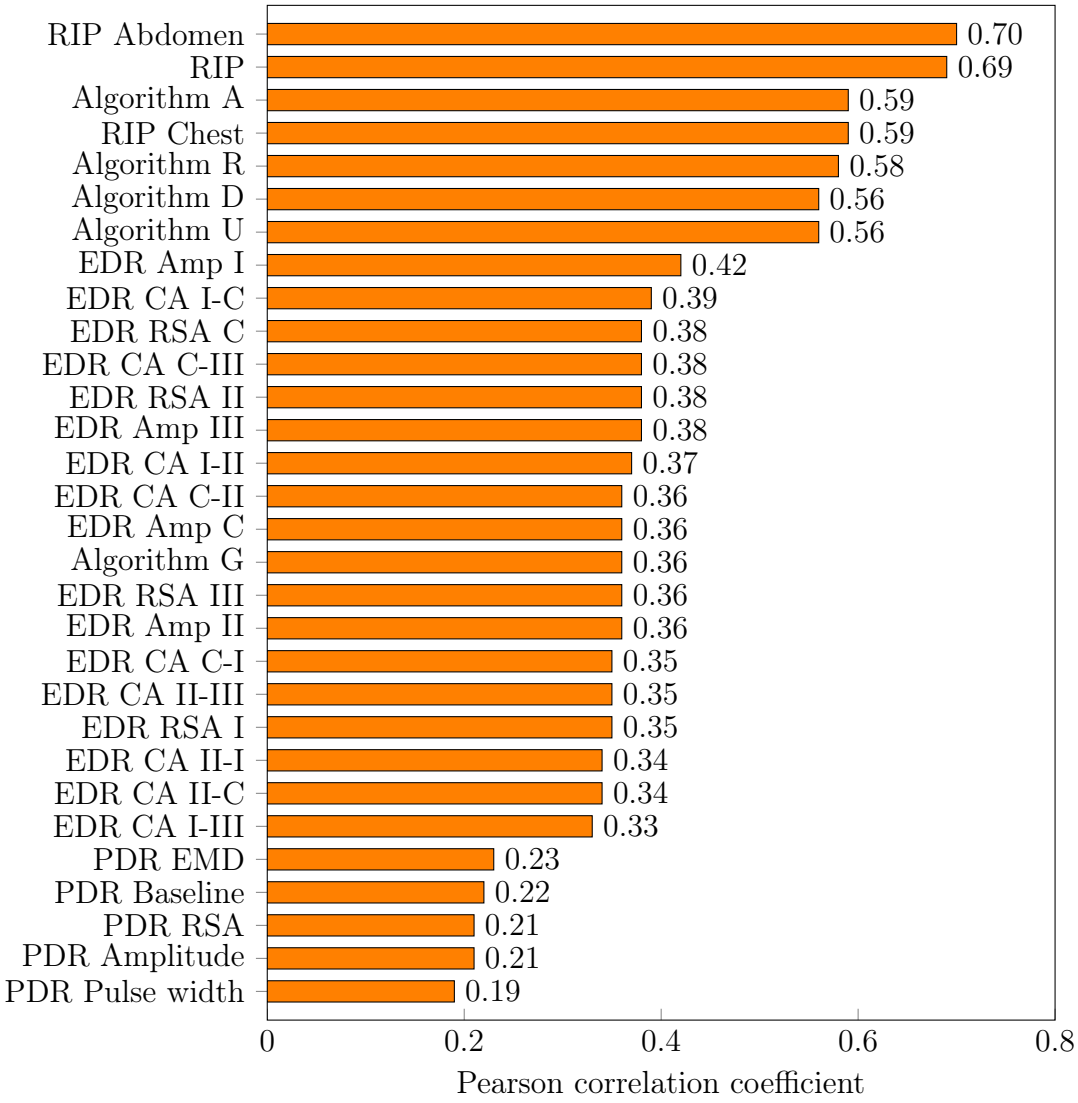

Figure 26: Pearson correlation coefficients of all evaluated methods.

4.1.6 Overall performance of evaluated methods

All evaluated methods are ranked based on the performance measures and each method is assigned a rank number which can be summed over all measures to acquire the order of overall performance as presented in Table 5.

According to these results, RIP technology outperforms IP, but the gain in performance should compensate for the increase in workload in order for RIP to replace the convenient impedance measurement. The RIP methods are followed by

Table 5: Rank numbers based on each performance measure and their sum as the overall performance ranking.

	Reliability	Bias	Accuracy	Precision	Correlation	Sum
RIP Abdomen	1	16	1	1	1	20
RIP	2	17	2	2	2	25
RIP Chest	4	15	3	4	4	30
Algorithm A	5	19	5	5	3	37
Algorithm D	6	18	4	3	6	37
Algorithm U	3	5	6	22	7	43
EDR Amp III	9	6	8	9	13	45
EDR Amp C	7	10	7	8	15	47
EDR Amp II	8	8	9	10	19	54
EDR CA C-III	14	7	12	13	11	57
EDR Amp I	13	12	15	17	8	65
EDR CA II-III	10	9	11	14	21	65
EDR CA C-I	12	14	10	11	20	67
EDR CA C-II	15	11	13	12	16	67
EDR CA I-C	19	2	18	21	9	69
EDR CA I-II	18	4	17	20	14	73
EDR CA II-C	17	1	16	16	24	74
EDR CA II-I	16	13	14	15	23	81
Algorithm R	11	20	21	30	5	87
Algorithm G	21	24	20	6	17	88
EDR CA I-III	20	3	19	23	25	90
EDR RSA C	25	26	25	7	10	93
EDR RSA II	22	25	23	18	12	100
EDR RSA III	24	23	24	19	18	108
EDR RSA I	23	22	22	24	22	113
PDR EMD	26	21	30	29	26	132
PDR Pulse width	27	27	26	26	30	136
PDR RSA	28	29	27	27	28	139
PDR Baseline	30	30	29	25	27	141
PDR Amplitude	29	28	28	28	29	142

Algorithms A, D, and U that perform significantly better than Algorithms R and G.

Amplitude-based EDR methods are more reliable, accurate, and precise than those based on RSA or cardiac angle. EDR method using the amplitude information from ECG lead I seem to perform worse than the other amplitude-based EDRs in terms of all performance measures except correlation which was the highest among EDR methods. This might arise from the fact that the respiratory amplitude modulation is not as well perceived from the direction of the lead I as it is from other leads.

The EDR methods based on cardiac angle are not as good as the amplitude-based but better than the RSA-based EDRs when considering the results of reliability and accuracy. In terms of bias, cardiac angle based methods are as good as amplitude-based. The reliability, accuracy, and precision of cardiac angle based methods were worse when the QRS-detection was conducted on the data from lead I instead of lead II or C.

In terms of reliability, bias, and accuracy the RSA-based methods are the worst among EDRs. Most of the RSA-based EDRs are more precise than the cardiac angle based methods with QRS-detection from lead I.

The ranking of EDR methods by correlation differs significantly from the rankings based on other performance measures. Based on the correlation coefficients alone, it would not be possible to determine which EDR approach is the most feasible. However, taking into account all results presented here, it seems that the amplitude-based EDR would be the most feasible option. Its performance is comparable to impedance measurements in terms of all calculated performance measures excluding correlation. RSA-based EDR methods perform poorer than the worst impedance algorithm. Thus, it is unlikely that these methods could be used to improve respiratory rate measurement in a multi-parameter application.

The PDR EMD method differs from the other PDR methods in terms of the calculated performance metrics, especially by bias and precision, whereas the rest resulted in very similar values. Considering the overall performance of evaluated PDR methods, it is safe to say that all PDR methods evaluated here perform equally poorly rendering them all unfit for use in a real application with moving patients.

4.2 Activity evaluation

Naturally the performance of respiratory rate measurements decrease when the patient moves and the signals become disturbed by motion. The effect of different activities on the reliability of the methods was analysed together with violations of alarm limits during the same activities. When both reliability and alarm criteria were evaluated simultaneously the results were dominated by reliability criterion. This means than the reliability of the methods is more affected by motion than alarm performance. In addition to the effect of activities, the effect of acceleration was assessed independent of the context of motion.

4.2.1 Reliability

The percentages of time when RR was reliably measured during each activity were averaged over groups of methods and presented in Table 6. Group Algorithms contains all impedance algorithms including Algorithm U. Amplitude, cardiac angle, and RSA-based EDR methods were grouped separately, whereas all PDR methods formed one group.

In general, the reliability of most methods decreased during more active tasks. The activities during which the reliability of most methods dropped below 50% include walking with and without crutches, brushing teeth, moving on the bed or more precisely rolling from side to side on the bed, climbing and descending stairs, raising and decreasing the end of the bed 45 degrees, eating and drinking on the bed, reading on the bed, talking or using a pad while sitting on the bed, sitting on a wheel chair, lying on the bed while assistant moves it, and shaving.

On average the impedance algorithms measured RR reliably most of the time. The activities during which the reliability dropped below 50% include all the challenging activities listed above plus combing hair and running on a treadmill.

On average the reliability of amplitude-based EDR methods suffers during fewer activities than that of impedance algorithms, regardless that the overall reliability of some algorithms is slightly superior to that of these EDRs. Furthermore, the performance of amplitude-based EDR methods seems to be less affected by motion than the other method groups. Especially during eating and drinking, using a pad while sitting, combing hair, shaving, walking up and down the stairs or walking and running on a treadmill amplitude-based EDRs proved more reliable than impedance algorithms. It seems that when the patient is still or moving their hands the impedance algorithms are more reliable, but once the patient is upright and moving the reliability of amplitude-based EDRs is often higher. This means that integrating the amplitude-based EDR with impedance measurements might result in a more reliable ambulatory solution than impedance alone.

The cardiac angle based EDRs are also sometimes more reliable during activities including walking than impedance algorithms. However, the reliability of amplitude-based EDRs is almost always slightly better than that of cardiac angle based methods. RSA-based EDR and PDR methods are unreliable during almost all of the activities. When the volunteers were just lying still, these methods were able to measure RR reliably about half of the time, but with increasing activity the reliability decreases substantially, especially for PDR methods. The reliability of PDR methods did not exceed that of impedance algorithms during any activity. RSA-based EDRs managed to do this notably only during running.

The most reliable methods throughout all activities are by far the RIP methods. The most challenging activities for these were moving on the bed, raising and decreasing the bed, eating and drinking, talking, and brushing teeth. For some reason also walking to the staircase and standing still was more challenging for RIP methods than any other walking related task, including walking in the stairs. Nevertheless, the RIP outperformed all other methods during most activities which suggest that RIP alone might actually be more reliable than any possible multi-

Table 6: The percentages of time when RR was reliably measured during each activity averaged over groups of methods. Values less than 50% on bold.

Activity number	Short description of activity	Algo-rithms	EDR Amp	EDR CA	EDR RSA	PDR	RIP
1	Lying still, supine	80	57	51	55	**46**	79
2	Lying still, left side	59	59	**46**	55	**38**	79
3	Lying still, right side	74	65	57	55	**47**	77
4	Moving on the bed	**33**	**46**	**37**	**34**	**21**	**27**
5	Moving legs on the bed	54	67	58	**39**	**34**	57
6	Lying, bed moves	51	**47**	**42**	**26**	**34**	68
7	Lying, raising bed 45°	**44**	54	**43**	**35**	**32**	**35**
8	Reading	**32**	**42**	**44**	**28**	**25**	50
9	Half sitting	67	67	56	51	**27**	70
10	Sitting, hands up	72	**48**	52	**46**	**27**	56
11	Sitting, moving hands fast	78	54	**43**	**43**	**46**	75
12	Sitting, moving hands slow	88	57	**48**	**47**	**19**	82
13	Sitting, touching shoulders	83	66	64	**45**	51	91
14	Sitting, hand shaking	72	54	**44**	**34**	**38**	82
15	Sitting, eating and drinking	**45**	55	54	**23**	**17**	**25**
16	Sitting, talking	**45**	**39**	**48**	**37**	**16**	**43**
17	Sitting, using pad	**39**	52	**49**	**37**	**31**	53
18	Sitting, using hand muscles	57	53	55	**41**	**28**	68
19	Sitting still	52	57	58	**25**	**22**	52
20	Getting up, standing still	57	60	**39**	**13**	**24**	74
21	Walking	**32**	**46**	**45**	**28**	**7**	57
22	Walking with crutches	**46**	**41**	**43**	**49**	**24**	68
23	Sitting still	**43**	50	**49**	**42**	**12**	64
24	Sitting, chair moves	64	53	**45**	**49**	**30**	74
25	Brushing teeth	**40**	**48**	**38**	**26**	**1**	**36**
26	Combing hair	**35**	67	60	**27**	**4**	67
27	Shaving	**46**	65	**42**	**28**	**13**	73
28	Walking, standing still	**32**	**36**	**39**	**14**	**9**	**41**
29	Climbing stairs	**38**	**41**	**42**	**10**	**8**	69
30	Standing still	**39**	**48**	**45**	**14**	**10**	58
31	Descending stairs	**37**	**47**	51	**19**	**18**	75
32	Standing still	**39**	**45**	**43**	**25**	**17**	65
33	Climbing stairs, handrail	**46**	62	58	**30**	**19**	76
34	Standing still	**45**	62	58	**37**	**13**	73
35	Descending stairs, handrail	**38**	54	**45**	**17**	**22**	81
36	Standing still	**37**	51	**44**	**17**	**12**	61
37	Walking on treadmill	51	59	57	**31**	**18**	89
38	Running on treadmill	**44**	66	59	58	**16**	91
39	Decreasing the bed	**38**	**41**	**41**	**21**	**21**	**43**
40	Lying still	86	60	53	54	53	90

parameter approach combining the other methods evaluated here. It is not in the scope of this thesis to make conclusions whether IP should be replaced with RIP in the future, but the acquired results give good reason to re-consider the choice of technology when developing a completely new respiratory monitoring solution.

4.2.2 Alarm performance

Alarm fatigue is a serious problem in hospitals, especially when clinicians feel that some measurements generate so many alarms that they prefer not to measure in the first place or silence the alarms and then miss a fatal one. For this reason, alarm breaches are detected during each activity to assess what kind of activities cause low or high RR alarms. The alarms limits were 5 and 30 brpm for low and high RR, respectively. During some activities the true RR may exceed these limits in which case the calculation is correct. However, these alarms are unwanted if the patient is fine and moving. Here activities that caused RR to be outside of normal range were identified. This information could be used for example together with accelerometer data to silence alarms that are generated as a result of certain activity in order to improve the alarms performance of RR measurements.

The percentage the measured RR was inside alarm limits was calculated for each method during each activity. Alarm performances for similar types of methods were so similar that the percentages could be averaged over the same groups of methods as used in the previous section. These averaged results and presented in Table 7. Among impedance algorithms, the Algorithm R had a worse alarms performance than the other algorithms, which manifested during walking, staircase activities, and running. EDR Amp I and III also had a worse alarm performance than the EDR Amp II and C especially during different hand movements while sitting. The same applies to EDR CA I-X and EDR RSA I methods. It is logical that the ECG lead I would be most affected by raising and moving hands as the skin under the arm electrodes stretches. Among the PDR methods, the EMD method breaches alarm limits more often than the other methods. The RIP abdomen belt has a slightly better alarm performance than the chest belt.

When comparing all methods together it is obvious that the RIP has the best alarm performance as it very rarely exceeds the limits. EDR methods are on the same level with impedance algorithms when it comes to alarms. The difference is that EDR methods are slightly worse during hand movements due to the interference on lead I, but compensate during some walking and running activities. The alarm performance of PDR methods is significantly worse than that of other methods.

It is no surprise that activities such as walking, climbing the stairs, and running cause measured RR to rise above the limit as it is likely that the volunteer was actually breathing fast. It is not known how long it takes for breathing to normalise after such activities. This might explain why alarm limits were exceeded during activities right after walking or running, such as standing still, sitting down, and sitting still while assistant pushes the wheel chair. However, it is somewhat curious why there is a clear drop in alarm performance during lying in hospital bed while assistant moves the bed around.

Table 7: The percentages of time when RR was inside alarm limits during each activity averaged over groups of methods. Values less than 80% on bold.

Activity number	Short description of activity	Algo-rithms	EDR Amp	EDR CA	EDR RSA	PDR	RIP
1	Lying still, supine	100	100	100	98	89	99
2	Lying still, left side	97	97	96	97	80	97
3	Lying still, right side	99	100	100	99	84	98
4	Moving on the bed	97	100	99	99	99	99
5	Moving legs on the bed	100	100	100	100	94	100
6	Lying, bed moves	93	83	88	84	93	100
7	Lying, raising bed 45°	100	96	97	95	**78**	100
8	Reading	100	96	97	94	82	100
9	Half sitting	100	100	100	99	**64**	100
10	Sitting, hands up	100	98	98	97	**65**	98
11	Sitting, moving hands fast	100	90	95	98	85	100
12	Sitting, moving hands slow	100	93	94	92	89	100
13	Sitting, touching shoulders	100	97	97	96	87	100
14	Sitting, hand shaking	100	92	93	94	88	100
15	Sitting, eating and drinking	100	97	95	98	87	100
16	Sitting, talking	100	100	100	100	**70**	100
17	Sitting, using pad	100	99	95	94	80	100
18	Sitting, using hand muscles	100	100	100	100	87	100
19	Sitting still	98	100	100	97	**57**	100
20	Getting up, standing still	98	96	95	86	**49**	100
21	Walking	**66**	**78**	**78**	**78**	**69**	96
22	Walking with crutches	86	89	90	90	88	100
23	Sitting still	86	89	88	88	84	100
24	Sitting, chair moves	89	81	82	81	**46**	100
25	Brushing teeth	96	86	**76**	86	**33**	97
26	Combing hair	99	100	98	100	**42**	100
27	Shaving	99	96	91	91	**30**	100
28	Walking, standing still	83	**78**	**78**	**78**	**48**	100
29	Climbing stairs	80	**78**	**77**	**78**	**62**	96
30	Standing still	**73**	**77**	**76**	**75**	**52**	99
31	Descending stairs	**78**	**79**	**79**	**79**	**69**	88
32	Standing still	**71**	**78**	**78**	**78**	**71**	99
33	Climbing stairs, handrail	80	90	89	89	**72**	99
34	Standing still	**79**	88	86	89	**57**	100
35	Descending stairs, handrail	**75**	81	80	80	**74**	100
36	Standing still	**69**	**78**	**78**	**78**	**67**	100
37	Walking on treadmill	**74**	99	88	99	**57**	98
38	Running on treadmill	**57**	82	80	**65**	**29**	81
39	Decreasing the bed	**71**	**69**	**67**	**71**	**64**	89
40	Lying still	98	96	95	92	**76**	97

The occurrence of alarms should not be a problem for EDR methods if alarm delays are used, but PDR methods would most likely burden clinicians with nuisance alarms. Alarms during walking or running could also be prevented if there was a way to detect these activities. Such a feature could be based on acceleration information, but was unavailable for this thesis.

4.2.3 Prediction probabilities

Motion artefact appear in physiological signals when the subject of measurements moves. Assuming that acceleration data could help identify when motion artefacts are present, there would most likely have to be a certain threshold above which the acceleration would yield a noisy signal resulting in unreliable RR measurement. One reason for calculating prediction probabilities was to explore whether such a threshold exists.

Table 8 presents the calculated prediction probabilities. A P^K value of 1 would mean that always when the acceleration value increases also the error would increase, indicating that the performance of the method is directly dependent on the level of acceleration. A value of 0.5 would mean that there is only 50% chance that an increase in acceleration would increase the error. A value close to 0.5 also means that it would be difficult to find a limit of acceleration that could reliably identify when RR measurement is unreliable.

Based on the P^K values the performance of evaluated methods does not seem to be directly linked to the level of acceleration. The highest prediction probability values are associated to Algorithms R and U, PDR EMD, and Algorithm G. These methods are not the most sensitive to motion, but the level of acceleration explains the level of errors better for these than for the other methods.

According to these results, acceleration explain errors only a little better than pure chance. Due to this reason, all attempts tested during algorithm development to utilize acceleration information in order to improve the performance of evaluated methods were unsuccessful. It seems that the relationship between motion and motion artefacts in the signals processed here is not directly linked to acceleration. Using accelerometer data in context detection might be a better approach than using some acceleration value directly. For example, detecting when the patient is standing or walking might better help to identify when motion artefacts are causing longer lasting effects on the signals. Further research is required to determine how acceleration information could be utilized in a multi-parameter respiratory rate measurement. Acceleration derived respiration methods were out of the scope of this thesis, but have great potential, if there is the possibility to fix an accelerometer to the torso of the patient.

4.3 Reliability of acquired results

There are various factors that may have contributed to the results acquired. The performances of all methods were evaluated against the reference which was always assumed to represent the true respiration. However, the reference measurement was

Table 8: Average prediction probabilities.

	P^K
Algorithm A	0.57
Algorithm D	0.56
Algorithm G	0.60
Algorithm R	0.67
Algorithm U	0.62
EDR Amp I	0.53
EDR Amp II	0.53
EDR Amp III	0.52
EDR Amp C	0.51
EDR CA I-II	0.51
EDR CA I-III	0.51
EDR CA I-C	0.51
EDR CA II-I	0.53
EDR CA II-III	0.52
EDR CA II-C	0.50
EDR CA C-I	0.53
EDR CA C-II	0.50
EDR CA C-III	0.49
EDR RSA I	0.54
EDR RSA II	0.56
EDR RSA III	0.57
EDR RSA C	0.57
PDR Amplitude	0.57
PDR Baseline	0.58
PDR EMD	0.61
PDR Pulse width	0.58
PDR RSA	0.58
RIP Abdomen	0.55
RIP Chest	0.56
RIP	0.55

capnography through a nasal cannula which is susceptible to missed breaths, if the volunteer accidentally breathes through the mouth instead of the nose. In order to minimize possible inaccuracies originating from this weakness the volunteers were instructed to breathe through the nose during the whole test.

The impedance algorithms are not all directly comparable as they return differently calculated RR values. Algorithm A returns only averaged RR values, Algorithm G produces a new RR value only once per minute, and the others return both instantaneous and differently averaged values. The outputs were processed in a way

that they were as comparable as possible. When an algorithm returned instantaneous RR values, the output signal was averaged by calculating a new RR value every 10 seconds over a window of the last 30 seconds. The output of the Algorithm A was averaged in the same manner regardless of the fact that the output was already averaged. This increased the performance of the algorithm in terms of all performance measures except bias. The output of the Algorithm G was simply interpolated over the whole recording from values that were provided less frequently. The sparsely calculated RR values might explain why Algorithm G performed significantly worse than the other impedance algorithms.

Even though RR was calculated in a similar manner for all methods except the Algorithms A and G, the universal Algorithm U was optimized for each method to maximize reliability and accuracy. Overfitting is a possible problem with this approach since the optimization was conducted for the whole dataset used in this work. The size of the available dataset was so small that it was not divided into test and validation sets but used as a whole. Cross-validation could have been used to avoid the effect of overfitting. The consequence of this decision is that the results can not be generalized into a wider dataset and the performances would most likely decrease if the analysis was reproduced on different data.

The poor performance of all PDR methods was unexpected. Previously pulse oximetry-derived respiratory rate has been measured from spontaneously breathing and relaxed general care floor patients with bias of -0.48 and precision of 1.77 brpm [68]. The results acquired here were significantly worse, but some deterioration is of course to be expected when the protocol contains a myriad of activities. Attempts to use the raw PPG waveform were doomed as the baseline of the raw signal was extremely sensitive to motion. Thus, a filtered signal was used instead. The drawback of this decision was that the baseline-based PDR was calculated from a filtered signal where the original baseline was no longer present and the resulting PDR signal was not in fact based on the baseline modulation of the PPG waveform but more connected to the amplitude modulation. The amplitude and RSA-based modulations still remain in the filtered signal.

5 Conclusions

This thesis described the development and feasibility evaluation of multi-parameter respiratory rate measurements. The feasibility of EDR and PDR methods was assessed by statistical analysis of different performance measures and by taking into account the effect of different activities on the performance.

One goal of this thesis was to identify the conditions when IP performs unreliably. Activities that cause the IP measurement to work unreliably more than half of the time include walking, running, rolling around on the bed and reading. In general, motion decreases the reliability of impedance algorithms as well as most of the methods evaluated here. However, it was found that motion does not affect the amplitude-based, and also cardiac angle based, EDR methods as much as IP or the other derived methods. In other words, these EDR methods seemed to be less sensitive to motion than IP.

The overall performance of impedance algorithms is better than that of the derived methods evaluated here. Nevertheless, the amplitude-based EDR methods were able to outperform IP in almost all of the situations where the reliability of IP was compromised. Thus, a multi-parameter approach combining impedance with EDR in the calculation of respiratory rate should be more robust during different activities than IP alone.

The amplitude-based EDRs were found more reliable than the cardiac angle based EDR methods which in turn outperformed the RSA-based EDR methods evaluated here. Due to this clear order of superiority among the different EDR approaches the amplitude-based EDR methods should be prioritized over the other EDRs in future development.

The overall performance of all PDR methods was found so poor that all PDR methods were considered unfit for use in an ambulatory solution due to high susceptibility to motion. The analysis did not identify any conditions in which the PDR methods would have performed better than IP. Thus, it is very unlikely that including these methods into a multi-parameter respiratory rate measurement could add any value.

The future development of multi-parameter respiratory rate algorithm would require a way to choose when to use different methods and to combine these together in the best way. There is a need for more research focusing on the use of accelerometer data to determine when to use another method, such as the amplitude-based EDR, instead of or together with IP. One way would be to use accelerometer data in context detection to identify at least when the patient is lying, upright, walking or otherwise moving around. A common approach to use multiple data sources simultaneously is to calculate an average weighted by some weighting coefficient for each data source. For example, the calculation could be based only on IP when the patient is lying and only on amplitude-based EDR when accelerometer detects that the patient is moving. Based on the results acquired here, this kind of solution should produce more reliable RR measurement than impedance alone. Acceleration information could also help to improve the alarm performance of IP.

Although this thesis did not focus on comparing IP and RIP technologies, it was

confirmed that the overall performance of RIP is superior to IP also in the presence of different activities. Especially activities like walking and running caused considerably more deterioration in IP compared to RIP. In fact, the results gave evidence to believe that RIP might be more reliable than any multi-parameter approach combining the other methods evaluated here. This raises the question whether RIP would be the best option for ambulatory respiration monitoring as it is notably more robust than any other method evaluated here. Does the increase in reliability of respiratory rate monitoring justify the use of a completely new piece of measurement equipment or would the use of RIP belts be too much work for the clinicians when IP is already available via ECG electrodes? This is something that should be considered in the future.

References

[1] L. Clifton, D. A. Clifton, P. J. Watkinson, and L. Tarassenko, "Identification of patient deterioration in vital-sign data using one-class support vector machines," in *2011 Federated Conference on Computer Science and Information Systems, FedCSIS 2011*, pp. 125–131, 2011.

[2] R. Schein, N. Hazday, M. Pena, B. Ruben, and C. Sprung, "Clinical antecedents to in-hospital cardiopulmonary arrest," *Chest*, vol. 98, no. 6, pp. 1388–1392, 1990.

[3] J. Tirkkonen, J. Nurmi, and S. Hoppu, "Sairaalansisäinen ensihoito on tullut jäädäkseen," *Duodecim*, vol. 130, pp. 2311–2317, 2014.

[4] S. Pannick, I. Beveridge, R. Wachter, and N. Sevdalis, "Improving the quality and safety of care on the medical ward: A review and synthesis of the evidence base," *European Journal of Internal Medicine*, vol. 25, no. 10, pp. 874–887, 2014.

[5] M. Buist, E. Jarmolowski, P. Burton, S. Bernard, B. Waxman, and J. Anderson, "Recognising clinical instability in hospital patients before cardiac arrest or unplanned admission to intensive care. a pilot study in a tertiary-care hospital," *Medical Journal of Australia*, vol. 171, no. 1, pp. 22–25, 1999. Abstract.

[6] M. DeVita, G. Smith, S. Adam, I. Adams-Pizarro, M. Buist, R. Bellomo, R. Bonello, E. Cerchiari, B. Farlow, D. Goldsmith, H. Haskell, K. Hillman, M. Howell, M. Hravnak, E. Hunt, A. Hvarfner, J. Kellett, G. Lighthall, A. Lippert, F. Lippert, R. Mahroof, J. Myers, M. Rosen, S. Reynolds, A. Rotondi, F. Rubulotta, and B. Winters, ""identifying the hospitalised patient in crisis"-a consensus conference on the afferent limb of rapid response systems," *Resuscitation*, vol. 81, no. 4, pp. 375–382, 2010.

[7] R. Bellomo, M. Ackerman, M. Bailey, R. Beale, G. Clancy, V. Danesh, A. Hvarfner, E. Jimenez, D. Konrad, M. Lecardo, K. S. Pattee, J. Ritchie, K. Sherman, and P. Tangkau, "A controlled trial of electronic automated advisory vital signs monitoring in general hospital wards," *Critical Care Medicine*, vol. 40, pp. 2349–2361, 2012.

[8] M. Boniatti, N. Azzolini, D. da Fonseca, B. Ribeiro, V. de Oliveira, R. Castilho, M. Raymundi, R. Coelho, and E. Filho, "Prognostic value of the calling criteria in patients receiving a medical emergency team review," *Resuscitation*, vol. 81, no. 6, pp. 667–670, 2010.

[9] C. Subbe, R. Davies, E. Williams, P. Rutherford, and L. Gemmell, "Effect of introducing the modified early warning score on clinical outcomes, cardiopulmonary arrests and intensive care utilisation in acute medical admissions," *Anaesthesia*, vol. 58, pp. 797–802, 2003.

[10] M. Cretikos, R. Bellomo, K. Hillman, J. Chen, S. Finfer, and A. Flabouris, "Respiratory rate: The neglected vital sign," *Medical Journal of Australia*, vol. 188, no. 11, pp. 657–659, 2008.

[11] P. Barthel, R. Wensel, A. Bauer, A. Müller, P. Wolf, K. Ulm, K. Huster, D. Francis, M. Malik, and G. Schmidt, "Respiratory rate predicts outcome after acute myocardial infarction: A prospective cohort study," *European Heart Journal*, vol. 34, no. 22, pp. 1644–1650, 2013.

[12] P. Berghuis, N. Cohen, M. Decker, A. Gettinger, K. Myrabo, J. Nilsestuen, K. Strohl, and J. Yount, *Biophysical measurement series: Respiration*. SpaceLabs, 1992.

[13] G. Harrison, T. Jacques, G. Kilborn, and M.-L. McLaws, "The prevalence of recordings of the signs of critical conditions and emergency responses in hospital wards - the soccer study," *Resuscitation*, vol. 65, no. 2, pp. 149–157, 2005.

[14] B. Jones, "Developing a vital sign alert system," *American Journal of Nursing*, vol. 113, no. 8, pp. 36–44, 2013.

[15] L. Lynn and J. Curry, "Patterns of unexpected in-hospital deaths: A root cause analysis," *Patient Safety in Surgery*, vol. 5, no. 1, 2011.

[16] A. Sovijärvi, A. Uusitalo, E. Länsimies, and I. Vuori, eds., *Kliininen fysiologia*. Kustannus Oy Duodecim, 1st ed., 1994.

[17] M. G. Levitzky, *Pulmonary physiology*. McGraw-Hill, 4th ed., 1995.

[18] R. M. Kacmarek, D. Hess, and J. K. Stoller, *Monitoring in Respiratory Care*, ch. Impedance Pneumography, Apnea Monitoring, and Respiratory Inductive Plethysmography, pp. 479–493. Mosby, 1993.

[19] A. Gaucher, D. Frasca, O. Mimoz, and B. Debaene, "Accuracy of respiratory rate monitoring by capnometry using the capnomask® in extubated patients receiving supplemental oxygen after surgery," *British Journal of Anaesthesia*, vol. 108, no. 2, pp. 316–320, 2012.

[20] V.-P. Seppä, J. Viik, and J. Hyttinen, "Assessment of pulmonary flow using impedance pneumography," *IEEE Transactions on Biomedical Engineering*, vol. 57, pp. 2277–2285, 2010.

[21] J. Rosell and J. Webster, "Signal-to-motion artifact ratio versus frequency for impedance pneumography," *IEEE Transactions on Biomedical Engineering*, vol. 42, no. 3, pp. 321–323, 1995.

[22] J. Freundlich and J. Erickson, "Electrical impedance pneumography for simple nonrestrictive continuous monitoring of respiratory rate, rhythm and tidal volume for surgical patients," *CHEST*, vol. 65, no. 2, pp. 181–184, 1974.

[23] V.-P. Seppä, M. Uitto, and J. Viik, "Tidal breathing flow-volume curves with impedance pneumography during expiratory loading," in *Proceedings of the Annual International Conference of the IEEE Engineering in Medicine and Biology Society, EMBS*, pp. 2437–2440, 2013.

[24] J. Wilkinson and V. Thanawala, "Thoracic impedance monitoring of respiratory rate during sedation - is it safe?," *Anaesthesia*, vol. 64, no. 4, pp. 455–456, 2009.

[25] V.-P. Seppä, J. Viik, A. Naveed, J. Väisänen, and J. Hyttinen, "Signal waveform agreement between spirometer and impedance pneumography of six chest band electrode configurations," in *IFMBE Proceedings*, vol. 25, pp. 689–692, 2009.

[26] K. Davidson, A. Bersten, T. Nicholas, P. Ravenscroft, and I. Doyle, "Measurement of tidal volume by using transthoracic impedance variations in rats," *Journal of Applied Physiology*, vol. 86, no. 2, pp. 759–766, 1999.

[27] N. Donnelly, T. Hunniford, R. Harper, A. Flynn, A. Kennedy, D. Branagh, and J. McLaughlin, "Demonstrating the accuracy of an in-hospital ambulatory patient monitoring solution in measuring respiratory rate," in *Proceedings of the Annual International Conference of the IEEE Engineering in Medicine and Biology Society, EMBS*, pp. 6711–6715, 2013.

[28] N. Taccini, G. Loriga, M. Pacelli, and R. Paradiso, "Wearable monitoring system for chronic cardio-respiratory diseases," in *Proceedings of the 30th Annual International Conference of the IEEE Engineering in Medicine and Biology Society, EMBS'08 - "Personalized Healthcare through Technology"*, pp. 3690–3693, 2008.

[29] P. Fiedler, S. Biller, S. Griebel, and J. Haueisen, "Impedance pneumography using textile electrodes.," in *Proceedings of the Annual International Conference of the IEEE Engineering in Medicine and Biology Society.*, vol. 2012, pp. 1606–1609, 2012.

[30] N. Khambete, P. Metherall, B. Brown, R. Smallwood, and R. Hose, "Can we optimize electrode placement for impedance pneumography?," *Annals of the New York Academy of Sciences*, vol. 873, pp. 534–542, 1999.

[31] J. Malmivuo and R. Plonsey, *Bioelectromagnetism*, ch. 25. Impedance plethysmography, pp. 405–419. Oxford University Press, 1995.

[32] V.-P. Seppä, J. Hyttinen, and J. Viik, "A method for suppressing cardiogenic oscillations in impedance pneumography," *Physiological Measurement*, vol. 32, no. 3, pp. 337–345, 2011.

[33] L. Arnson, J. Rau Jr., and R. Dixon, "Evaluation of two electronic respiratory rate monitoring systems.," *Respiratory Care*, vol. 26, no. 3, pp. 221–227, 1981.

[34] Y. Huang, M. Young, and C. Tai, "Noninvasive respiratory monitoring system based on the piezoceramic transducer's pyroelectric effect," *Review of Scientific Instruments*, vol. 79, no. 3, 2008.

[35] Y.-P. Huang and K.-N. Huang, "Monitoring of breathing rate by a piezofilm sensor using pyroelectric effect," in *ICOT 2013 - 1st International Conference on Orange Technologies*, pp. 99–102, 2013.

[36] P. Janik, M. Janik, and Z. Wróbel, "Micro-condensation sensor for monitoring respiratory rate and breath strength," *Sensors and Actuators, A: Physical*, vol. 185, pp. 160–167, 2012.

[37] H. Pettersson, E. Stenow, H. Cai, and P. Öberg, "Optical aspects of a fibre-optic sensor for respiratory rate monitoring," *Medical & Biological Engineering & Computing*, vol. 34, no. 6, pp. 448–452, 1996.

[38] O. Mimoz, T. Benard, A. Gaucher, D. Frasca, and B. Debaene, "Accuracy of respiratory rate monitoring using a non-invasive acoustic method after general anaesthesia," *British Journal of Anaesthesia*, vol. 108, no. 5, pp. 872–875, 2012.

[39] M. Patino, D. Redford, T. Quigley, M. Mahmoud, C. Kurth, and P. Szmuk, "Accuracy of acoustic respiration rate monitoring in pediatric patients," *Paediatric Anaesthesia*, vol. 23, no. 12, pp. 1166–1173, 2013.

[40] B. Popov, G. Sierra, V. Telfort, R. Agarwal, and V. Lanzo, "Estimation of respiratory rate and heart rate during treadmill tests using acoustic sensor," in *Annual International Conference of the IEEE Engineering in Medicine and Biology - Proceedings*, vol. 7 VOLS, pp. 5884–5887, 2005.

[41] T. Sogabe, K. Uriu, K. Fujii-Abe, K. Ashigaki, K. Doushita, S. Sekita, and H. Kawahara, "Monitoring of acoustic respiration rate during intravenous sedation for dental treatment in disabled persons," *Journal of Japanese Dental Society of Anesthesiology*, vol. 43, no. 1, pp. 17–21, 2015.

[42] D. Frasca, L. Geraud, J.-M. Charriere, B. Debaene, and O. Mimoz, "Comparison of acoustic and impedance methods with mask capnometry to assess respiration rate in obese patients recovering from general anaesthesia," *Anaesthesia*, vol. 70, no. 1, pp. 26–31, 2015.

[43] A. Droitcour, T. Seto, B.-K. Park, S. Yamada, A. Vergara, C. El Hourani, T. Shing, A. Yuen, V. Lubecke, and O. Boric-Lubecke, "Non-contact respiratory rate measurement validation for hospitalized patients," in *Proceedings of the 31st Annual International Conference of the IEEE Engineering in Medicine and Biology Society: Engineering the Future of Biomedicine, EMBC 2009*, pp. 4812–4815, 2009.

[44] J. Andre and P. Mendes, "Development of a rf contactless respiratory rate monitor," in *3rd Portuguese Bioengineering Meeting, ENBENG 2013 - Book of Proceedings*, 2013.

[45] F.-F. Jiang, X. Wang, D. Yang, and J.-J. Jin, "Research on detection method of respiratory rate based on ballistocardiogram signal," *Xitong Fangzhen Xuebao / Journal of System Simulation*, vol. 23, no. 11, pp. 2357–2360, 2011.

[46] A. Bates, M. Ling, J. Mann, and D. Arvind, "Respiratory rate and flow waveform estimation from tri-axial accelerometer data," in *2010 International Conference on Body Sensor Networks, BSN 2010*, pp. 144–150, 2010.

[47] P. Dehkordi, M. Marzencki, K. Tavakolian, M. Kaminska, and B. Kaminska, "Validation of respiratory signal derived from suprasternal notch acceleration for sleep apnea detection," in *Proceedings of the Annual International Conference of the IEEE Engineering in Medicine and Biology Society, EMBS*, pp. 3824–3827, 2011.

[48] G. Liu, Y. Guo, Q. Zhu, B. Huang, and L. Wang, "Estimation of respiration rate from three-dimensional acceleration data based on body sensor network.," *Telemedicine journal and e-health : the official journal of the American Telemedicine Association*, vol. 17, no. 9, pp. 705–711, 2011.

[49] A. Chan, N. Ferdosi, and R. Narasimhan, "Ambulatory respiratory rate detection using ecg and a triaxial accelerometer," in *Proceedings of the Annual International Conference of the IEEE Engineering in Medicine and Biology Society, EMBS*, pp. 4058–4061, 2013.

[50] G.-Z. Liu, D. Wu, Z.-Y. Mei, Q.-S. Zhu, and L. Wang, "Automatic detection of respiratory rate from electrocardiogram, respiration induced plethysmography and 3d acceleration signals," *Journal of Central South University*, vol. 20, no. 9, pp. 2423–2431, 2013.

[51] L. Zhao, S. Reisman, and T. Findley, "Derivation of respiration from electrocardiogram during heart rate variability studies," in *Computers in Cardiology 1994*, pp. 53–56, Sep 1994.

[52] A. Travaglini, C. Lamberti, J. DeBie, and M. Ferri, "Respiratory signal derived from eight-lead ecg," in *Computers in Cardiology*, vol. 25, pp. 65–68, 1998.

[53] E. Helfenbein, R. Firoozabadi, S. Chien, E. Carlson, and S. Babaeizadeh, "Development of three methods for extracting respiration from the surface ecg: A review," *Journal of Electrocardiology*, 2014. Article in Press.

[54] G. B. Moody, R. G. Mark, A. Zocola, and S. Mantero, "Derivation of respiratory signals from multi-lead ecgs.," in *Computers in Cardiology*, pp. 113–116, 1985.

[55] D. Caggiano and S. Reisman, "Respiration derived from the electrocardiogram: a quantitative comparison of three different methods," in *Bioengineering, Proceedings of the Northeast Conference*, pp. 103–104, 1996.

[56] D. Dobrev and I. Daskalov, "Two-electrode telemetric instrument for infant heart rate and apnea monitoring," *Medical Engineering and Physics*, vol. 20, no. 10, pp. 729–734, 1999.

[57] G. Furman, Z. Shinar, A. Baharav, and S. Akselrod, "Electrocardiogram derived respiration during sleep," in *Computers in Cardiology*, vol. 32, pp. 351–354, 2005.

[58] S. Arunachalam and L. Brown, "Real-time estimation of the ecg-derived respiration (edr) signal using a new algorithm for baseline wander noise removal.," *Conference proceedings : ... Annual International Conference of the IEEE Engineering in Medicine and Biology Society. IEEE Engineering in Medicine and Biology Society. Conference*, pp. 5681–5684, 2009.

[59] D. Cysarz, R. Zerm, H. Bettermann, M. Frühwirth, M. Moser, and M. Kröz, "Comparison of respiratory rates derived from heart rate variability, ecg amplitude, and nasal/oral airflow," *Annals of Biomedical Engineering*, vol. 36, no. 12, pp. 2085–2094, 2008.

[60] P. Langley, E. Bowers, and A. Murray, "Principal component analysis as a tool for analyzing beat-to-beat changes in ecg features: Application to ecg-derived respiration," *IEEE Transactions on Biomedical Engineering*, vol. 57, no. 4, pp. 821–829, 2010.

[61] C. Shannon, "Communication in the presence of noise," *Proceedings of the IRE*, vol. 37, no. 1, pp. 10–21, 1949.

[62] R. Bailón, L. Sörnmo, and P. Laguna, "A robust method for ecg-based estimation of the respiratory frequency during stress testing," *IEEE Transactions on Biomedical Engineering*, vol. 53, no. 7, pp. 1273–1285, 2006.

[63] D. Widjaja, C. Varon, A. Dorado, J. Suykens, and S. Van Huffel, "Application of kernel principal component analysis for single-lead-ecg- derived respiration," *IEEE Transactions on Biomedical Engineering*, vol. 59, no. 4, pp. 1169–1176, 2012.

[64] S. Tiinanen, K. Noponen, M. Tulppo, A. Kiviniemi, and T. Seppänen, "Ecg-derived respiration methods: Adapted ica and pca," *Medical Engineering and Physics*, vol. 37, no. 5, pp. 512–517, 2015.

[65] D. Labate, F. Foresta, G. Occhiuto, F. Morabito, A. Lay-Ekuakille, and P. Vergallo, "Empirical mode decomposition vs. wavelet decomposition for the extraction of respiratory signal from single-channel ecg: A comparison," *IEEE Sensors Journal*, vol. 13, no. 7, pp. 2666–2674, 2013.

[66] H. Sharma, K. Sharma, and O. Bhagat, "Respiratory rate extraction from single-lead ecg using homomorphic filtering," *Computers in Biology and Medicine*, vol. 59, pp. 80–86, 2015.

[67] P. Addison, J. Watson, M. Mestek, and R. Mecca, "Developing an algorithm for pulse oximetry derived respiratory rate (rroxi): A healthy volunteer study," *Journal of Clinical Monitoring and Computing*, vol. 26, no. 1, pp. 45–51, 2012.

[68] P. Addison, J. Watson, M. Mestek, J. Ochs, A. Uribe, and S. Bergese, "Pulse oximetry-derived respiratory rate in general care floor patients," *Journal of Clinical Monitoring and Computing*, vol. 29, no. 1, pp. 113–120, 2014.

[69] J. Lázaro, E. Gil, R. Baión, A. Mincholé, and P. Laguna, "Deriving respiration from photoplethysmographic pulse width," *Medical and Biological Engineering and Computing*, vol. 51, no. 1-2, pp. 233–242, 2013.

[70] S. Dash, K. H. Shelley, D. G. Silverman, and K. H. Chon, "Estimation of respiratory rate from ecg, photoplethysmogram, and piezoelectric pulse transducer signals: A comparative study of time-frequency methods," *IEEE Transactions on Biomedical Engineering*, vol. 57, no. 5, pp. 1099–1107, 2010.

[71] A. Garde, W. Karlen, P. Dehkordi, J. Ansermino, and G. Dumont, "Empirical mode decomposition for respiratory and heart rate estimation from the photoplethysmogram," in *Computing in Cardiology*, vol. 40, pp. 799–802, 2013.

[72] N. Huang, S. Shen, M. Long, H. Wu, Q. Shih, N.-C. Zheng, C. Tung, and H. H. Liu, "The empirical mode decomposition and the hilbert spectrum for non-linear and non stationary time series analysis," *Proceedings of the Royal Society of London A*, vol. 454, pp. 903–995, 1998.

[73] O. Such, "Motion tolerance in wearable sensors–the challenge of motion artifact.," *Proceedings of the 29th Annual International Conference of the IEEE Engineering in Medicine and Biology Society. Conference*, pp. 1542–1545, 2007.

[74] A. Lanata, E. Scilingo, E. Nardini, G. Loriga, R. Paradiso, and D. De-Rossi, "Comparative evaluation of susceptibility to motion artifact in different wearable systems for monitoring respiratory rate," *IEEE Transactions on Information Technology in Biomedicine*, vol. 14, no. 2, pp. 378–386, 2010.

[75] S. Luo, V. Afonso, J. Webster, and W. Tompkins, "The electrode system in impedance-based ventilation measurement," *IEEE Transactions on Biomedical Engineering*, vol. 39, no. 11, pp. 1130–1141, 1992.

[76] M. Mayotte, J. Webster, and W. Tompkins, "A comparison of electrodes for potential use in paediatric/infant apnoea monitoring," *Physiological Measurement*, vol. 15, no. 4, pp. 459–467, 1994.

[77] M. Mayotte, J. Webster, and W. Tompkins, "Reduction of motion artefacts during paediatric/infant apnoea monitoring," *Medical and Biological Engineering and Computing*, vol. 34, no. 1, pp. 93–96, 1996.

[78] N. Khambete, B. Brown, and R. Smallwood, "Movement artefact rejection in impedance pneumography using six strategically placed electrodes," *Physiological Measurement*, vol. 21, no. 1, pp. 79–88, 2000.

[79] Z. Zhang, I. Silva, D. Wu, J. Zheng, H. Wu, and W. Wang, "Adaptive motion artefact reduction in respiration and ecg signals for wearable healthcare monitoring systems," *Medical and Biological Engineering and Computing*, vol. 52, no. 12, pp. 1019–1030, 2014.

[80] J. Rosell, K. Cohen, and J. Webster, "Reduction of motion artifacts using a two-frequency impedance plethysmograph and adaptive filtering," *IEEE Transactions on Biomedical Engineering*, vol. 42, no. 10, pp. 1044–1048, 1995.

[81] A. Schäfer and K. Kratky, "Estimation of breathing rate from respiratory sinus arrhythmia: Comparison of various methods," *Annals of Biomedical Engineering*, vol. 36, no. 3, pp. 476–485, 2008.

[82] W. Smith, R. Dutton, and T. Smith, "Measuring the performance of anesthetic depth indicators," *Anesthesiology*, vol. 84, no. 1, pp. 38–51, 1996.

A Test protocols

This appendix describes in detail the protocols used in both preliminary and primary data collections. The preliminary data collection was conducted in Helsinki by the author of this thesis with two volunteers, while the primary data was collected from ten volunteers by VTT in Tampere.

Preliminary data collection

Measurement 1:

1. Supine position: free breathing
2. Sitting position: free breathing
3. Standing position: free breathing
4. Standing position: free breathing

Measurement 2:

1. Supine position
   (a) Free breathing
   (b) 5 breaths slightly slower than normal
   (c) 5 breaths as slowly as possible
   (d) 5 free breaths
   (e) 5 breaths slightly faster than normal
   (f) 5 breaths as fast as possible
   (g) Free breathing
   (h) 5 breaths as deep as possible
   (i) 5 breaths as shallow as possible
   (j) 5 increasingly deep breaths
   (k) 5 increasingly shallow breaths
   (l) 5 abdominal breaths
   (m) 5 chest breaths
   (n) Couching twice
   (o) Counting out loud from 1 to 10
   (p) Free breathing
   (q) Inspiration and simulated central apnea
   (r) Free breathing
   (s) Expiration and simulated central apnea
   (t) Free breathing
   (u) Inspiration and simulated obstructed apnea
   (v) Free breathing

(w) Expiration and simulated obstructed apnea

2. Lying on left side: repeat a-w
3. Sitting position: repeat a-o
4. Half sitting position: repeat a-o
5. Standing position: repeat a-o
6. Walking: repeat a-o

Measurement 3:

1. Supine position
   (a) Free breathing
   (b) Free breathing without mask
   (c) Free breathing
   (d) 5 breaths as fast as possible
   (e) 5 breaths slightly faster than normal
   (f) 5 free breaths slightly slower than normal
   (g) 5 breaths as slow as possible
   (h) Free breathing
   (i) 2 breaths as deep as possible
   (j) 2 breaths as shallow as possible
   (k) 5 increasingly deep breaths
   (l) 5 increasingly shallow breaths
   (m) 5 abdominal breaths
   (n) 5 chest breaths
   (o) Couching twice
   (p) 2 free breaths
   (q) Counting out loud from 1 to 10
   (r) Free breathing
   (s) Inspiration and simulated central apnea
   (t) Free breathing
   (u) Expiration and simulated central apnea
   (v) Free breathing
   (w) Inspiration and simulated obstructed apnea
   (x) Free breathing
   (y) Expiration and simulated obstructed apnea
2. Lying on left side: repeat a-y
3. Sitting position: repeat a-q

Measurement 4:

1. Half sitting position: same than Measurement 3 a-q
2. Standing position: repeat a-q
3. Walking: repeat a-q

Measurement 5:

1. Supine position
   (a) Fast breathing
   (b) Slow breathing
   (c) Deep breathing
   (d) Shallow breathing
   (e) Fast and deep breathing
   (f) Fast and shallow breathing
   (g) Slow and deep breathing
   (h) Slow and shallow breathing
   (i) Talking
2. Lying on left side: repeat a-i
3. Sitting position: repeat a-i
4. Standing position: repeat a-i

Measurement 6:

1. Sitting position
   (a) 4 deep and fast breaths
   (b) Eating an apple
   (c) Drinking
   (d) 4 deep and fast breaths

Primary data collection

Syncing

1. Syncing Caremonitor and plethy: tap ECG electrodes with plethy finger (30 s)
2. Syncing Faros and plethy: tap Faros with plethy finger (30 s)
3. Syncing resp: 5 deep breaths (30 s)
4. Syncing accelerometers: jump 5 times (30 s)
5. Syncing: Caremonitor and Faros lead off (30 s)

Activities

1. Lying still on the bed on back + BP (5 min)
2. Lying still on the bed on left side + BP (2 min)
3. Lying still on the bed on right side + BP (2 min)
4. Moving on the bed (imagine that cannot get sleep or having pain) (1 min)
5. Lying on the bed on back, bend and straighten legs repetitively (1 min)
6. Assistant pushes the bed + BP (1 min)
7. Raising the bed 45° (1 min)
8. Reading a book on the bed + BP (1 min)
9. Sitting still on the bed in half sitting position (45° angle) + BP (2 min)
10. Sitting on the bed, raising hands above the head and keeping hands up + BP (1 min)
11. Sitting on the bed, hands in front of the body in 90° and turning palms (fast pace) + BP (1 min)
12. Sitting on the bed, hands in front of the body in 90° and turning palms slow pace (1 per 5 sec) + BP (1 min)
13. Sitting on the bed, touching shoulders with hands repetitively (1 min)
14. Sitting on the bed, shake(small) plethy hand (tremor) (1 min)
15. Sitting on the bed, eating and drinking (1 min)
16. Sitting on the bed and having a discussion + BP (1 min)
17. Sitting on the bed and surfing on the Internet with pad (1 min)
18. Sitting on the bed pressing "hand muscle device" with both hands + BP (1 min)
19. Sitting on the edge of the bed hands still + BP (1 min)
20. Getting up from the bed and standing still + BP (1 min)
21. Walking around the lab + BP (2 min)
22. Walking around the lab with the crutches + BP (2 min)
23. Sitting down on the wheel chair, sitting hands still (30 s)
24. Assistant moving the chair + BP (2 min)
25. Brushing teeth + BP (2 min)
26. Combing hair (1 min)
27. Shaving (1 min)
28. Walking to the staircase and standing still (1 min)
29. Climbing the stairs not using the handrail + BP (2 min)
30. Standing still on top of the staircase (30 s)

31. Coming down the stairs and not using the handrail (2 min)
32. Standing still on the bottom of the staircase (30 s)
33. Climbing the stairs and using the handrail (2 min)
34. Standing still on top of the staircase (30 s)
35. Coming down the stairs and using the handrail (2 min)
36. Standing still on the bottom of the staircase (30 s)
37. Walking on the treadmill slowly (4km/h) + BP (2 min)
38. Running on the treadmill moderate pace (7km/h) (2 min)
39. Decreasing the bed (1 min)
40. Lying on the bed + BP (3 min)

Syncing

1. Syncing 5 deep breaths (30 s)
2. Syncing accelerometers: jump 5 times (30 s)
3. Syncing Caremonitor and plethy: tap ECG electrodes with plethy finger (30 s)
4. Syncing Faros and plethy: tap Faros with plethy finger (30 s)
5. Syncing: Caremonitor and Faros lead off (30 s)
6. End of recording (5 s)